基于单脉冲雷达和差通道多普勒估计的前视成像(中文/English)

李悦丽*① 马萌恩① 赵崇辉*② 周智敏①
①(国防科技大学电子科学学院 长沙 410073)
②(毫米波遥感技术重点实验室 北京 100854)

摘 要：单脉冲测角技术用于扫描雷达前视成像可有效提高图像的清晰度，但单个脉冲对同分辨单元多目标测角时会发生角闪烁现象，造成图像模糊。该文提出了一种基于单脉冲雷达和差通道多普勒估计的前视成像算法，利用目标和平台之间相对运动引起的多普勒梯度差异实现同分辨单元内不同方向目标的分离，然后在多普勒域采用和差比幅测角(SDAC)技术测量目标的方位角，完成能量投影。为提高测角精度，进一步提出了采用调频Z变换(CZT)重建和差多普勒估计并进行比幅测角的算法。点目标仿真实验结果表明，所提出的算法在前斜视方向具有分离多目标的能力，对实测数据成像结果验证了基于CZT的成像算法相比传统算法能显著提高对场景成像的轮廓清晰度。

关键词：单脉冲雷达；前视成像；和差比幅测角；调频Z变换
中图分类号：TN958.4 **文献标识码**：A **文章编号**：2095-283X(2021)01-0131-12
DOI: 10.12000/JR20111

引用格式：李悦丽, 马萌恩, 赵崇辉, 等. 基于单脉冲雷达和差通道多普勒估计的前视成像[J]. 雷达学报, 2021, 10(1): 131–142. doi: 10.12000/JR20111.

Reference format: LI Yueli, MA Meng'en, ZHAO Chonghui, *et al*. Forward-looking Imaging via Doppler estimates of sum-difference measurements in scanning monopulse radar[J]. *Journal of Radars*, 2021, 10(1): 131–142. doi: 10.12000/JR20111.

Forward-looking Imaging via Doppler Estimates of Sum-difference Measurements in Scanning Monopulse Radar (in English)

LI Yueli*① MA Meng'en① ZHAO Chonghui*② ZHOU Zhimin①
①(*College of Electronic Science and Technology, National University of Defense Technology, Changsha* 410073, *China*)
②(*Science and Technology on Millimeter-wave Laboratory, Beijing* 100854, *China*)

Abstract: Monopulse technique is used in scanning radar systems to improve image quality in the forward-looking area. However, monopulse measurements fail to resolve multiple targets in the same resolution cell because of angular glint which often results to image blurring. In response to this, we propose a monopulse forward-looking imaging method utilizing Doppler estimates of sum-difference measurements. First, target multiplicity is resolved by exploiting the different Doppler shifts caused by the relative motion between the platform and the targets at different directions. High azimuthal angle measurement accuracy of the Doppler estimates is then obtained using the Sum-Difference Amplitude-Comparison (SDAC) monopulse technique. Subsequently, the intensity of the sum channel estimates is projected onto the image plane according to the range and angle measurements. To further improve the precision of angle measurements, a Chirp-Z Transform (CZT)-based algorithm is proposed for the reconstruction of the Doppler estimates of the sum-difference

收稿日期：2020-08-01；改回日期：2020-10-27；网络出版：2020-11-16
*通信作者： 李悦丽 liyueli4uwb@nudt.edu.cn； 赵崇辉 zhaochonghui@163.com
*Corresponding Author: LI Yueli, liyueli4uwb@nudt.edu.cn; ZHAO Chonghui, zhaochonghui@163.com
基金项目：国家部委基金(61404150103, 61425020604)
Foundation Items: The National Pre-Research Foundation (61404150103, 61425020604)
责任主编：朱岱寅 Corresponding Editor: ZHU Daiyin

channels. Simulation results demonstrate the capability of the proposed methods in resolving multiple targets at high squint angles in a large scanning field. Real data experiments show significant improvement of image profiles using the CZT-based algorithm compared to that of the conventional monopulse imaging method.

Key words: Monopulse radar; Forward-looking imaging; Sum-Difference Amplitude Comparison (SDAC); Chirp-Z Transform (CZT)

1 引言

高分辨前视成像(High Resolution Forward-Looking Imaging, HRFLI)是指对飞行器正前方区域进行二维微波高分辨成像，一直以来都是雷达遥感领域的前沿技术难题，并已成为当前对地观测成像技术的研究热点[1]。目前前视成像的主要研究方向包括：双基地合成孔径雷达(Synthetic Aperture Radar, SAR)成像，超分辨(Super Resolution, SR)成像和单脉冲测角(Monopulse Technique, MT)成像。基于单基地雷达波束扫描模式的前视成像技术可用于机扫、相扫雷达，其中超分辨前视成像技术将天线波束对场景的扫描视为目标的雷达截面积与天线方向图的卷积，通过方位向回波和天线方向图实现目标超分辨成像，国内电子科技大学对扫描波束锐化的理论方法和实现技术进行了深入研究，并已在机载雷达上验证了高倍数的角度超分辨能力[2]；南京航空航天大学等机构对机载雷达扫描波束单脉冲成像的实现技术和聚焦性能进行了深入研究，并基于实测数据验证了该技术对特定场景的分辨率改善性能以及自聚焦成像算法[3–5]；我们最早研究基于单脉冲雷达和差通道的解卷积波束锐化技术[6]，由于单脉冲雷达通道方向图不严格满足强互质条件，在解卷积运算中会带来高频噪声放大问题，哈工大学者引入了ℓ_1正则化技术有效抑制了噪声[7]。

单脉冲成像技术具有系统复杂度低、对航迹无特殊要求的优点，是一种实际可行的前视成像方法，但是由于单脉冲测角的通道数限制，无法区分同分辨单元内多个目标并会导致“角闪烁”现象，从而造成对非稀疏场景的成像质量下降。Sherman等人[8]曾系统地研究了单脉冲测角中对多目标分辨的问题，指出两个任意目标和传统单脉冲天线方向图的条件下，单个脉冲不可能解决不可分辨目标问题；但是，当脉间存在波束指向、频率或极化变化时，有可能实现两个以上独立目标的分辨。对单脉冲雷达同分辨单元多目标分辨的一种思路是采用最大似然估计法构造和、差通道多次测量值的联合方程，然后用最优化方法得到目标参数估计，这种方法可实现天线波束内4个以下目标参数估计[9,10]，但联合最大似然估计的运算复杂度高，用于实时成像可行性有待验证；另一思路是基于目标的多普勒差异在多普勒域实现多目标分辨，最早用于多普勒波束锐化(Doppler Beam Sharpen, DBS)技术，通过主瓣内目标的多普勒中心差异提高图像分辨率[11]，西安电子科技大学陈伯孝等人[12–14]研究了单脉冲逆合成孔径雷达(Inverse Synthetic Aperture Radar, ISAR)三维成像技术，提出运用超分辨技术在多普勒域提高目标分辨性能，并指出APES(Amplitude and Phase EStimation)算法比快速傅里叶变换(Fast Fourier Transform, FFT)算法具有更高的多普勒分辨率，这一技术思路应用于扫描雷达前视对地成像中可望解决多目标带来的测角模糊问题，但仍需要克服前视区域目标多普勒梯度下降带来的问题。

为解决扫描前视成像时单脉冲雷达同分辨单元内多目标难以分辨导致的成像质量下降问题，本文提出了基于单脉冲雷达和差通道多普勒估计的前视成像方法。首先利用前斜视方向目标回波的多普勒梯度差异实现对多目标的分离，然后基于和差通道的多普勒估计值对目标进行和差比幅测角，根据距离和方位角将和通道的多普勒估计幅值投影到成像平面上得到前视图像。研究发现，目标和差通道的多普勒估计精度对测角性能影响很大，为此，进一步提出了基于调频Z变换的和差通道多普勒估计重建策略，具体方法是：对于和通道主瓣内多普勒单元中的目标，结合调频Z变换(Chirp-Z Transform, CZT)对频谱细化并搜索局部最大值，得到目标的精确多普勒频率[15]，然后基于频率估计重建目标的差通道多普勒估计；最后，利用重建值完成比幅测角和能量投影。仿真实验和实测数据处理结果表明：相比传统单脉冲前视成像算法，基于单脉冲雷达和差通道多普勒估计的前视成像有效提高了雷达在前斜视向对多目标分辨的能力，采用重建多普勒估计测角进一步提高了目标的定位精度，提高了图像清晰度。

2 基于多普勒估计的单脉冲前视成像原理

搭载在运动平台上的单脉冲雷达以角速度ω对前视场景扫描，脉冲重复频率为f_{p}。假设经过脉冲压缩和运动补偿后，连续N个脉冲在某距离门内的方位和、差通道复信号矢量分别表示为$\boldsymbol{y}_\Sigma=[y_{\Sigma 1}\ y_{\Sigma 2}\ \cdots\ y_{\Sigma N}]^{\mathrm{T}}$，$\boldsymbol{y}_\Delta=[y_{\Delta 1}\ y_{\Delta 2}\ \cdots\ y_{\Delta N}]^{\mathrm{T}}\in\mathbb{C}_{N\times 1}$，其回波信号模型的矩阵形式为

$$\left.\begin{aligned}\boldsymbol{y}_\Sigma &= \boldsymbol{A}_\Sigma\boldsymbol{s}+\boldsymbol{n}_\Sigma\\ \boldsymbol{y}_\Delta &= \boldsymbol{A}_\Delta\boldsymbol{s}+\boldsymbol{n}_\Delta\end{aligned}\right\} \tag{1}$$

其中，$\boldsymbol{s}\in\mathbb{C}_{K\times1}$为天线波束内目标的雷达截面积(Radar Cross Section, RCS)在扫描网格上的分布，$\boldsymbol{A}_\Sigma,\boldsymbol{A}_\Delta\in\mathbb{C}_{N\times K}$分别为和差天线方向图对空间扫描构成的感知矩阵，$\boldsymbol{n}_\Sigma,\boldsymbol{n}_\Delta\in\mathbb{C}_{N\times1}$为和差通道复噪声信号矢量(为简化分析，假设两个通道的噪声均服从0均值、方差为σ的独立高斯分布)。设3 dB方位波束宽度为$\theta_{3\,\mathrm{dB}}$，N为雷达在扫描到一个方位上发射和接收的驻留脉冲数；$K=\lfloor\theta_{3\,\mathrm{dB}}f_\mathrm{p}/\omega\rfloor$为雷达扫描天线3 dB波束覆盖范围内发射和接收的脉冲数，因此通常$N\ll K$，式(1)是一个欠定方程组，对式(1)的求解属病态逆问题求解范畴。由于N个脉冲内的天线增益变化几乎可以忽略，无法通过解方程组式(1)直接求解目标RCS在方位上的分布。在这种条件下，对目标前视成像有两种技术途径：一种是利用单脉冲成像技术，通过比较和差通道的信号幅度或相位测量目标偏离天线对称轴线的程度实现更高精度的测角，然后将目标能量投影到成像平面上[3]，这种方法可显著缩小目标点扩展函数的方位分布范围，因此能够提高图像清晰度，但是不能分辨多目标[4]。另一种是DBS技术，利用了目标相对平台运动产生的多普勒梯度差异分离位于不同角度的目标，然后采用多普勒中心估计和杂波锁定技术估计目标方位角并进行能量投影实现波束的锐化[16,17]，但是其锐化比受到多普勒滤波器带宽f_p/N的限制，一般在斜视角30°～50°范围内，波束锐化比可以达到32倍，再继续增大斜视角，锐化比将随着主瓣内目标多普勒频率差异减小而急剧下降形成盲区[18]。

基于单脉冲雷达和差通道多普勒估计的前视成像方法将以上两种技术思路结合起来，首先对扫描雷达某一距离门的连续N个脉冲回波进行多普勒处理，利用目标的多普勒差异将位于不同方位的目标分离，解决同分辨单元内多目标混迭的问题，提高方位分辨率；然后，基于和差通道的多普勒估计值直接进行和差比幅测角，实现对目标方位角的精确测量，最终实现目标的定位和能量投影。

在单脉冲雷达波束扫描模式中，首先建立了基于多普勒估计值进行单脉冲测角的信号模型。同式(1)，设同距离门内连续N个采样值构成了对目标信号的一维均匀采样，令$\boldsymbol{a}_\mathrm{D}(\omega)\triangleq[1\ \mathrm{e}^{-\mathrm{j}\omega}\ \cdots\ \mathrm{e}^{-\mathrm{j}(N-1)\omega}]^\mathrm{T}$为导向矢量，$\omega\in[0,2\pi)$为多普勒频率，则由脉冲重复频率$f_\mathrm{p}$所确定的均匀多普勒域采样间隔为$\omega_n=2\pi n/N,n=0,1,\cdots,N-1$。定义在方位向对信号进行离散傅里叶变换(Discrete Fourier Transform, DFT)的Fourier基矩阵$\boldsymbol{A}_\mathrm{D}\triangleq[\boldsymbol{a}_\mathrm{D}(\omega_0)\ \boldsymbol{a}_\mathrm{D}(\omega_1)\cdots\boldsymbol{a}_\mathrm{D}(\omega_{N-1})]\in\mathbb{C}_{N\times N}$，则有

$$\boldsymbol{A}_\mathrm{D}=\begin{bmatrix}1 & 1 & \cdots & 1\\ 1 & \mathrm{e}^{-\mathrm{j}\omega_1} & \cdots & \mathrm{e}^{-\mathrm{j}\omega_{N-1}}\\ \vdots & \vdots & \ddots & \vdots\\ 1 & \mathrm{e}^{-\mathrm{j}(N-1)\omega_1} & \cdots & \mathrm{e}^{-\mathrm{j}(N-1)\omega_{N-1}}\end{bmatrix},$$
$$\omega_n=2\pi n/N,n=0,1,\cdots,N-1 \tag{2}$$

和差通道信号的多普勒估计$\boldsymbol{Y}_\Sigma,\boldsymbol{Y}_\Delta\in\mathbb{C}_{N\times1}$可表示为矩阵形式

$$\left.\begin{aligned}\boldsymbol{Y}_\Sigma &= \boldsymbol{A}_\mathrm{D}\boldsymbol{y}_\Sigma=\boldsymbol{A}_\mathrm{D}(\boldsymbol{A}_\Sigma\boldsymbol{s}+\boldsymbol{n}_\Sigma)=\boldsymbol{A}_\mathrm{D}\boldsymbol{A}_\Sigma\boldsymbol{s}+\boldsymbol{e}_\Sigma\\ \boldsymbol{Y}_\Delta &= \boldsymbol{A}_\mathrm{D}\boldsymbol{y}_\Delta=\boldsymbol{A}_\mathrm{D}(\boldsymbol{A}_\Delta\boldsymbol{s}+\boldsymbol{n}_\Delta)=\boldsymbol{A}_\mathrm{D}\boldsymbol{A}_\Delta\boldsymbol{s}+\boldsymbol{e}_\Delta\end{aligned}\right\} \tag{3}$$

DFT可采用FFT算法实现，$\boldsymbol{e}_\Sigma,\boldsymbol{e}_\Delta\in\mathbb{C}_{N\times1}$仍服从均值为0的复高斯白噪声分布，当$N\ll K$时，可以忽略在$N$个脉冲范围内各个方位目标对应的天线增益加权变化，这意味着对于位于某方位角θ的目标$s(\theta)$，$\boldsymbol{A}_\Sigma(\theta)$和$\boldsymbol{A}_\Delta(\theta)$在$N$个脉冲内基本不变，因此多普勒处理后对和差多普勒估计值进行比幅测角仍可以测量目标的方位角。同时，当不同目标间的多普勒频差大于f_p/N时，多普勒处理可将目标区分开，实现多目标分辨的能力。

接下来需要确定目标能量在多普勒域的分布范围，这一步骤类似DBS处理中的杂波锁定，需要计算和通道天线波束中心对应目标的多普勒中心频率以及和通道3 dB波束宽度覆盖范围内目标的多普勒带宽。如图1雷达扫描成像几何关系示意图所示，设雷达平台飞行遵循匀速直线运动，其前向飞行速度为v_x，侧向飞行速度为0，雷达天线波束在前视方向扫描，当前和通道天线波束中心对应的方位角为θ，俯仰角为β，则和通道天线波束中心对应目标的多普勒中心频率为

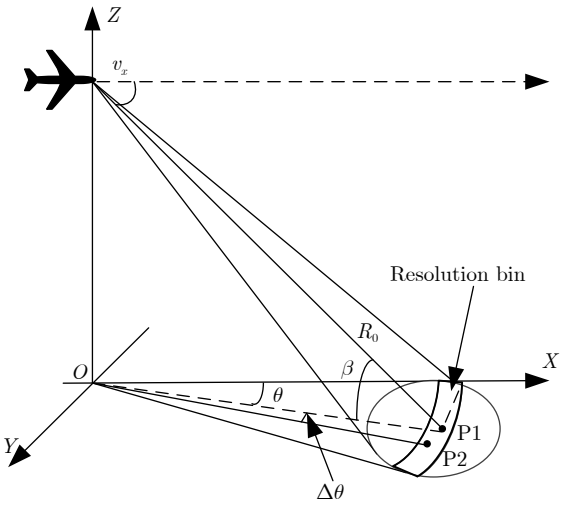

图 1 雷达扫描前视成像几何关系示意图

Fig. 1 Geometry for forward-looking imaging of a scanning radar

$$f_{\mathrm{DC}}=\frac{2v_x\cos\theta\cos\beta}{\lambda} \tag{4}$$

其中，λ为发射信号中心频率对应的波长，由$f_{\mathrm{DC}}/(f_{\mathrm{p}}/N)$确定天线波束中心对应地面目标的多普勒单元索引，此时如系统存在多普勒模糊，需要消除多普勒模糊的影响才能确定正确的索引。

在和通道天线波束覆盖区域中，若同一距离环带上、主瓣内两个目标P1和P2存在方位角偏差$\Delta\theta$，则两目标对应的多普勒中心频率频差Δf_{DC}为

$$\Delta f_{\mathrm{DC}}=f_{\mathrm{DC1}}-f_{\mathrm{DC2}}==\frac{2v_x\cos\beta\left[\cos\theta-\cos(\theta+\Delta\theta)\right]}{\lambda} \tag{5}$$

对于一般的天线波束，$\Delta\theta$很小，满足$\cos\Delta\theta\approx 1$, $\sin\Delta\theta\approx\Delta\theta$，则$\Delta f_{\mathrm{DC}}$可近似为

$$\Delta f_{\mathrm{DC}}=\frac{2}{\lambda}\cdot v_x\sin\theta\cdot\cos\beta\cdot\Delta\theta \tag{6}$$

因此，若和通道天线3 dB波束宽度在地面投影范围为$\theta_{3\ \mathrm{dB}}$，忽略多普勒调频率的影响，天线波束地面投影区域回波对应的多普勒带宽Δf_{D}为

$$\Delta f_{\mathrm{D}}\approx\frac{2}{\lambda}v_x\sin\theta\cdot\cos\beta\cdot\theta_{3\ \mathrm{dB}} \tag{7}$$

由$\Delta f_{\mathrm{D}}/(f_{\mathrm{p}}/N)$可以确定和通道天线3 dB波束范围内目标RCS在多普勒域的分布范围大小，结合式(4)确定的多普勒中心频率索引可得到3 dB波束内目标在多普勒域上的分布区域和对应多普勒单元索引。

设3 dB天线波束内的目标分布在M个多普勒单元内，根据多普勒单元索引在和差通道多普勒估计中提取各多普勒单元中的信号$\boldsymbol{Y}_{\Sigma}(\omega_m)$和$\boldsymbol{Y}_{\Delta}(\omega_m)$，完成和差通道复比$\varepsilon_m$[8]

$$\varepsilon_m=\mathrm{sgn}\left(\boldsymbol{Y}_{\Sigma\mathrm{I}}(\omega_m)\boldsymbol{Y}_{\Delta\mathrm{I}}(\omega_m)+\boldsymbol{Y}_{\Sigma\mathrm{Q}}(\omega_m)\boldsymbol{Y}_{\Delta\mathrm{Q}}(\omega_m)\right)\cdot\frac{|\boldsymbol{Y}_{\Delta}(\omega_m)|}{|\boldsymbol{Y}_{\Sigma}(\omega_m)|},\quad m=0,1,\cdots,M-1 \tag{8}$$

其中，sgn()表示求信号符号的函数，下标I和Q分别代表信号的实部和虚部，由ε_m在雷达鉴角曲线上对应查找到目标偏离中轴线的角度θ_e，则目标的真实方位角应为

$$\hat{\theta}_m=\theta-\theta_e \tag{9}$$

得到$\hat{\theta}_m$后，将该单元目标的和通道多普勒估计强度投影到对应的成像网格中进行能量积累，即可完成前视成像。

基于多普勒估计的单脉冲前视成像流程如图2所示，和差通道的原始回波在进行方位向处理前需完成脉冲压缩和距离走动校正，校正采用了Keystone算法[19]；校正后的回波在距离门内沿方位向分帧，然后对每一帧数据进行方位向FFT，得到和差通道的多普勒估计；接着，由平台运动参数计算3 dB波束内目标分布的多普勒单元索引，并提取对应的和差通道多普勒估计值计算和差信号的复比，得到目标的真实方位角；最后，根据目标所在的距离门和

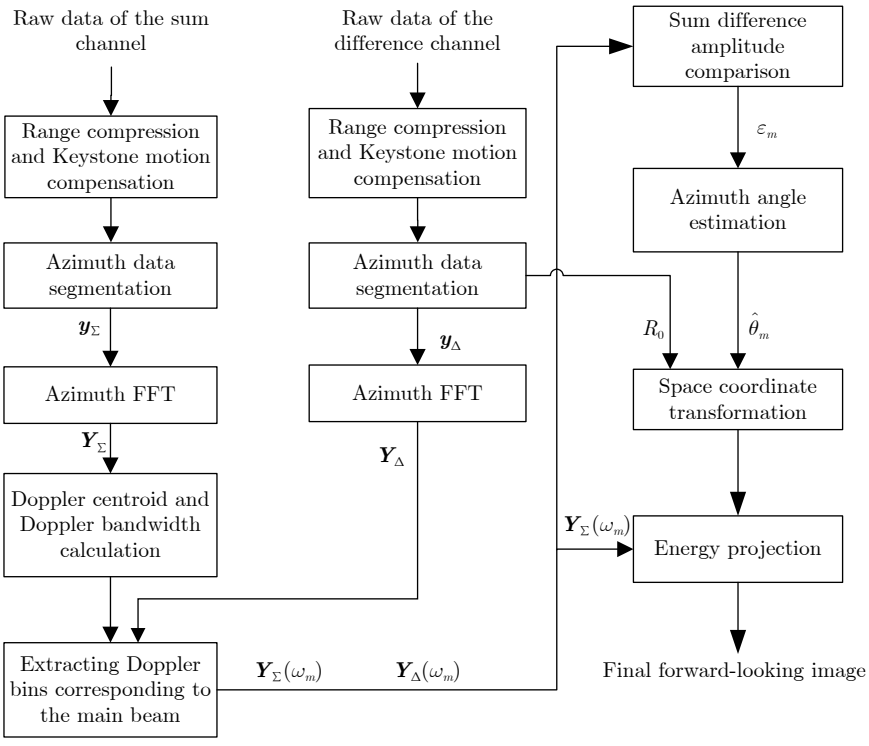

图 2 基于多普勒估计的单脉冲前视成像流程

Fig. 2 Flowchart of mono pulse forward-looking imagination based on Doppler estimates

方位角将和通道多普勒估计的强度作为目标能量投影到成像平面上，得到前视图像。

图2所示的成像流程中，成像是通过将目标能量投影到成像平面上实现的，因此对目标的定位精度(包括距离和方位角测量的精度)是影响成像质量的关键指标。研究发现，单脉冲测角技术对目标方位角测量的精度与目标回波信噪比(Signal to Noise Ratio, SNR)和目标偏离中轴线的角度有关，这一精度不会随着前斜视角度的减小而明显下降，所以相比同样基于多普勒处理的DBS技术，在前斜视方向采用单脉冲测角技术可以大大改善对目标定位精度，从而提高图像的清晰度。

3　基于调频Z变换重建单脉冲雷达和差通道多普勒估计值

上文分析表明，采用FFT算法对N个脉冲的样本值进行多普勒估计可实现前斜视方向上目标的分离，但是，也应注意到N的取值受到f_{p}或平台运动引起的相位误差等因素的限制，不能太大，这意味着用DFT构造的多普勒滤波器组，其分辨率在前斜视方向并不高，因此邻近目标的旁瓣或能量泄漏都可能会影响对目标的幅度估计结果，导致和差复比误差增大。为了提高对目标的定位精度，提出了一种基于调频Z变换重建单脉冲雷达和差通道多普勒估计值的算法。

由第2节可知，多普勒处理后，3 dB波束宽度内目标对应的多普勒单元为M个，首先对每个多普勒单元重新估计各单元内目标的多普勒频率。具体的方法是在每个目标所处多普勒单元附近采用CZT算法进行频率间隔细化，在细化后的多普勒估计值中搜索局部最大值，对应的频率即为目标的真实多普勒频率的估计[15]。设$\omega_m(i)$为第m个目标对应单元细化后的多普勒频率：

$$\omega_m(i)=\omega_0+i\frac{\Delta\omega}{L},\ m=0,1,\cdots,M-1;\quad i=0,1,\cdots,L-1 \tag{10}$$

其中，ω_0, $\Delta\omega$和L分别表示起始频率点、对频率间隔细化后的频率增量和细化后的样本点数，则细化后的频谱分辨率为$\Delta\omega/L$，与式(10)的频率样本集相对应的DFT应为

$$Y\left[\omega_m(i)\right]=\sum_{n=0}^{N-1}y(n)\mathrm{e}^{-\mathrm{j}\omega_m(i)n},\ i=0,1,\cdots,L-1 \tag{11}$$

若定义W为

$$W=\mathrm{e}^{-\mathrm{j}\frac{\Delta\omega}{L}} \tag{12}$$

则由式(11)、式(12)可得

$$Y\left[\omega_m(i)\right]=\sum_{n=0}^{N-1}y(n)\mathrm{e}^{-\mathrm{j}\omega_0 n}W^{ni},\ i=0,1,\cdots,L-1 \tag{13}$$

利用等式

$$ni=\frac{1}{2}\left[n^2+i^2-(i-n)^2\right] \tag{14}$$

式(13)可重写为

$$Y\left[\omega_m(i)\right]=\sum_{n=0}^{N-1}y(n)\mathrm{e}^{-\mathrm{j}\omega_0 n}W^{n^2/2}W^{i^2/2}W^{-(i-n)^2/2},\quad i=0,1,\cdots,L-1 \tag{15}$$

令

$$g(n)=y(n)\mathrm{e}^{-\mathrm{j}\omega_0 n}W^{n^2/2},\ \ n=0,1,\cdots,N \tag{16}$$

则可以得出

$$Y\left[\omega_m(i)\right]=W^{i^2/2}\left[\sum_{n=0}^{N-1}g\left(n\right)W^{-(i-n)^2/2}\right],\quad i=0,1,\cdots,L-1 \tag{17}$$

其中，$Y\left[\omega_m(i)\right]$是$g(n)$与$W^{-n^2/2}$两序列的卷积再与因子$W^{i^2/2}$相乘的结果，$W^{-n^2/2}$是以$n\Delta\omega/L$为线性频率增量上升的复指数序列，说明可以采用调频Z变换直接求得该目标的和通道多普勒估计$\boldsymbol{Y}_{\Sigma}\left(\omega_{mi}\right)$，然后找到峰值点所在的位置，即为目标的频率估计$\omega_{mr}$。基于目标的频率估计$\omega_{mr}$可以重建差通道的多普勒估计。首先，根据频率估计值$\omega_{mr}$构造导向矢量$\boldsymbol{a}_{\mathrm{D}}(\omega_{mr})\triangleq[1\ \mathrm{e}^{-\mathrm{j}\omega_{mr}}\ \cdots\ \mathrm{e}^{-\mathrm{j}(N-1)\omega_{mr}}]^{\mathrm{T}}$，然后用导向矢量乘以差通道原始的复信号矢量，求得差通道复信号在多普勒空间这一频率点上的投影，即为差通道的多普勒估计

$$\boldsymbol{Y}_{\Delta}(\omega_{mr})=\boldsymbol{a}_{\mathrm{D}}(\omega_{mr})^{\mathrm{T}}\boldsymbol{y}_{\Delta} \tag{18}$$

其中，重建使用的导向矢量相当于Fourier基矩阵中的一个列向量，区别在于频率更为精确，因此得到的和差估计值更接近目标的真实值，对目标测角的精度更高。接着，可由重建的和差多普勒估计计算和差通道复比ε_{mr}[8]

$$\varepsilon_{mr}=\mathrm{sgn}\left(\boldsymbol{Y}_{\Sigma\mathrm{I}}(\omega_{mr})\,\boldsymbol{Y}_{\Delta\mathrm{I}}(\omega_{mr})+\boldsymbol{Y}_{\Sigma\mathrm{Q}}\left(\omega_{mr}\right)\boldsymbol{Y}_{\mathrm{DQ}}\left(\omega_{mr}\right)\right)\cdot\frac{\left|\boldsymbol{Y}_{\Delta}\left(\omega_{mr}\right)\right|}{\left|\boldsymbol{Y}_{\Sigma}\left(\omega_{mr}\right)\right|} \tag{19}$$

然后根据和差通道鉴角曲线查询得到目标偏移中轴线的角度θ_e，根据式(9)即得到真实的方位角$\hat{\theta}_m$。

基于重建多普勒估计的单脉冲雷达前视成像流程如图3所示：首先，对和差通道的原始回波完成预处理，将Keystone校正后的和通道回波在距离门内沿方位向分成长度为N的子帧，然后用FFT处理子帧数据，得到和通道信号的多普勒估计；其次，根据雷达平台的运动参数计算多普勒中心频率和3 dB

波束内目标的多普勒带宽，确定目标在多普勒域的分布范围和单元索引；再次，用调频Z变换计算对应M个多普勒单元的精确多普勒估计以及多普勒频率，并重建差通道多普勒估计；然后，根据重建值计算目标的和差复比，利用雷达的鉴角曲线测角，得到目标的方位角；最后，根据各目标所在的距离门和方位角进行坐标变换，将目标和通道多普勒估计的幅值投影到成像平面上，得到前视图像。

4 仿真结果和算法性能分析

4.1 点目标阵列仿真实验

仿真参数如表1所示，假设雷达安装在机载平台上，发射脉宽1 μs、带宽50 MHz的线性调频信号，发射信号中心频率为18 GHz，设天线波束从–15°扫描到15°，发射的脉冲总数为2000个，在地面上以[0 m, 1700 m]为中心设置了3×21点目标阵列，点目标的强度均为1，在距离向和方位向间隔均为30 m，相邻点目标的方位角间隔约为1°，脉压后回波的SNR=20 dB，噪声服从均值为0，方差为σ^2的复正态分布。

经过预处理和运动补偿后，分别采用4种前视成像算法完成了信号处理，并绘制了等高线图，由于传统多普勒波束锐化在前斜视区域成像效果不佳，没有采用DBS算法进行对比。图4(a)为实孔径成像结果，成像分辨率很差。图4(b)为采用传统单脉冲成像算法的成像结果，距离分辨率保证了目标在距离上的有效分离，但是沿方位向目标之间发生了交叠，无法准确地确定各点目标的位置，说明同

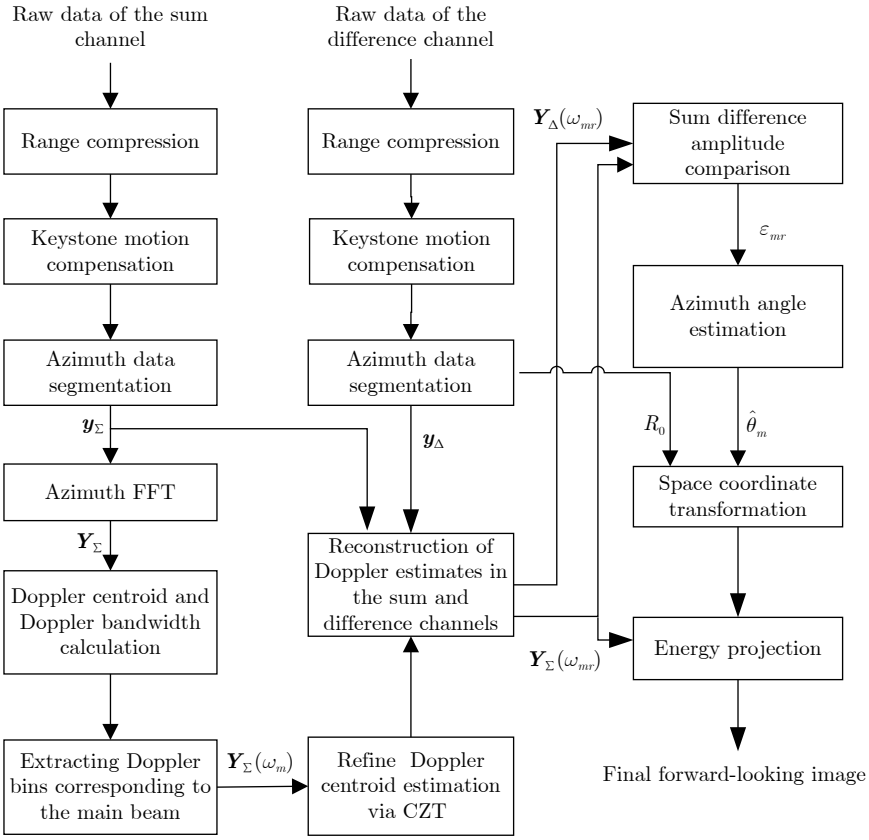

图 3 基于重建多普勒估计的单脉冲前视成像流程

Fig. 3 Flowchart of monopulse forward-looking imaging based on the reconstructed Doppler estimates

表 1 波束扫描前视成像实验仿真参数

Tab. 1 Simulation parameters of a forward-looking scanning radar

参数	取值	参数	取值
场景中心地距	1700 m	平台飞行速度	100 m/s
雷达中心频率	18 GHz	距离×方位分辨单元	3 m×3 m
信号带宽	50 MHz	信号脉宽	1 μs
和通道3 dB波束宽度	5°	波束扫描范围	–15°～15°
脉冲重复频率PRF	2000 Hz	天线扫描速度	30°/s

分辨单元内的多目标使得单脉冲测角不准确，引起了图像模糊。图4(c)采用图2给出的算法，图4(d)采用图3给出的算法，脉冲积累数N=64。在图4(c)中可以观察到靠左右两侧的点目标在方位向得到了分离，但同时目标周围散布着大量的杂波；图4(d)相比图4(c)，左右两侧点目标的方位分布范围明显缩小，距离向和方位向的背景杂波也明显减少。

为了对比图像中目标的方位分辨情况，在图5中绘制了图4(b)—图4(d)中在地距1730 m处21个目标的归一化方位向剖面图：图中红色圆圈代表目标的真实位置，绿色虚线绘制的是传统单脉冲前视成像得到的目标方位向剖面图，可观察到多数目标由于角闪烁偏离了真实位置；采用基于多普勒估计的单脉冲前视成像算法得到的目标方位向剖面图如蓝色虚线所示，方位向±200 m外目标偏离真实位置的程度下降明显，但是目标强度起伏和分裂也比较明显；采用重建多普勒估计的单脉冲前视成像算法得到的目标方位向剖面图如红色实线所示，相比其它曲线，在方位向±180 m外的目标位置与真实值吻合度很高，目标的方位分布更为集中，幅度也更均匀，显示算法对目标的方位分辨率明显提高。

同时，我们也注意到图4和图5中，在正前方两侧一定范围内存在一个目标混迭区，在此范围内目标的多普勒梯度受到斜视角的影响急剧下降，多个角度的目标落入同一个多普勒单元，导致算法失效。

4.2 场景仿真验证

证明了所提方法在稀疏场景重建上的有效性后，我们进一步研究了该方法用于重建扩展目标的可行性。由于扩展目标包含了大量强度相似的散射点，采用单脉冲成像技术时，相对于稀疏点目标场景重建的难度更大。

仿真中，我们采用了一幅Ku波段SAR图像作为原始场景，经过降采样处理后图像分辨率为3 m×3 m(如图6所示)，用于生成一个典型单脉冲雷达前视扫描的仿真回波数据。图像数据置于以[0 m, 1700 m]为中心的地面，对应的最大方位角为17°，天线波束扫描范围扩大为–20°到20°以确保波束可以覆盖目标，其余参数采用表1中的参数。成像结

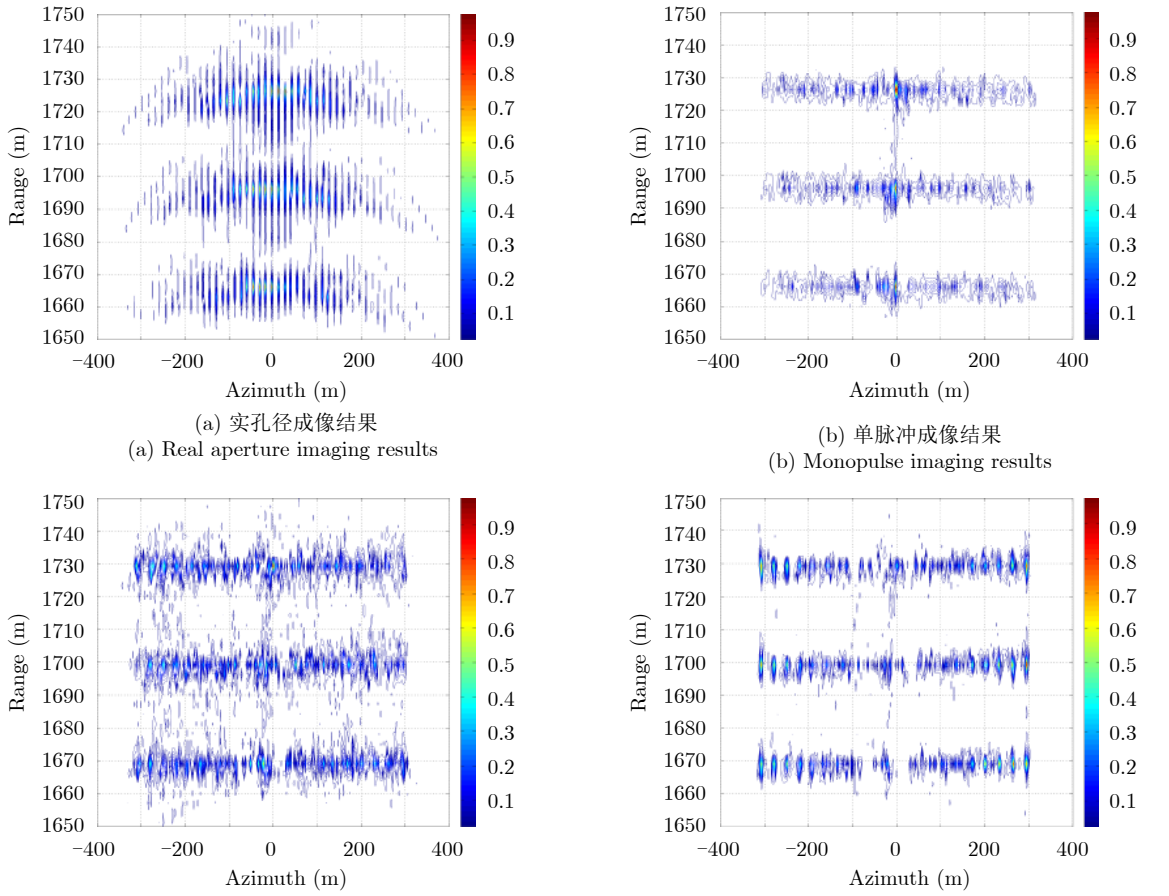

(a) 实孔径成像结果
(a) Real aperture imaging results

(b) 单脉冲成像结果
(b) Monopulse imaging results

(c) 基于FFT进行多普勒估计的单脉冲成像结果
(c) Monopulse imaging results based on Doppler estimates by using FFT

(d) 基于CZT重建多普勒估计的单脉冲成像结果
(d) Monopulse imaging results based on reconstructed Doppler estimates by using CZT

图 4 点阵目标单脉冲前视成像效果对比(SNR=20 dB)

Fig. 4 Comparison of forward-looking imaging performance (SNR=20 dB)

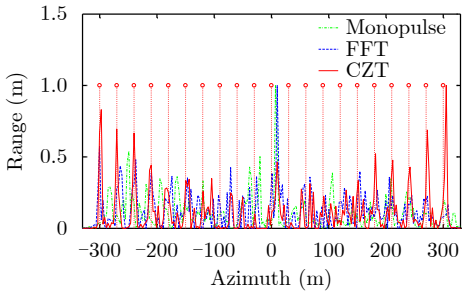

图 5 距离1730 m处目标的方位向剖面图(SNR=20 dB)

Fig. 5 Azimuthal contour plots for point targets at the range cell 1730 m (SNR=20 dB)

果用dB图表示，图6(b)所示为采用传统的单脉冲成像方法成像的结果，可以观察到由于角闪烁存在使得图像存在严重的模糊现象。图6(c)采用了基于多普勒估计的单脉冲前视成像算法，将和差通道数据的多普勒估计值用于估计波束扫描范围内散射点的波达方向，并把估计值按坐标变换结果投影成像。图6(c)中场景轮廓得到了有效重建，散射点分布与图6(a)基本一致。图6(d)为采用基于CZT重建和差多普勒估计的单脉冲前视成像结果，相比图6(c)，目标的轮廓更为清晰，背景杂波明显减少。进一步采用统计信杂比(Signal to Clutter Ratio, SCR)分析了成像的质量，统计SCR为目标区域内信号能量与杂波能量的比值，以dB为单位，即

$$\mathrm{SCR}=20\lg\left(\frac{S_{\mathrm{r}}}{C_{\mathrm{r}}}\right) \tag{20}$$

其中，S_{r}为截取的信号区域幅度均值，C_{r}为截取的杂波区域幅度均值。图6(a)中黄框对应位置为截取的信号区域，红框对应位置为截取的背景杂波区域，由于斑点噪声的存在，图6(a)原始场景统计意义上的SCR约为20.03 dB；图6(b)中得到的统计SCR为23.46 dB，尽管传统单脉冲成像的信杂比更高，但存在严重的图像失真，场景的边缘模糊；经过多普勒估计重建后的图6(c)和图6(d)的统计SCR分别为18.36 dB和22.45 dB。仿真结果表明，本文所提算法具有对扩展目标前视高分辨成像的潜力。

4.3 实测数据验证

图7是对某机载单脉冲雷达实测数据的前视成像处理结果，平台飞行过程中雷达对水面进行扫描，波束扫描范围为–24°～24°。雷达和通道天线3 dB

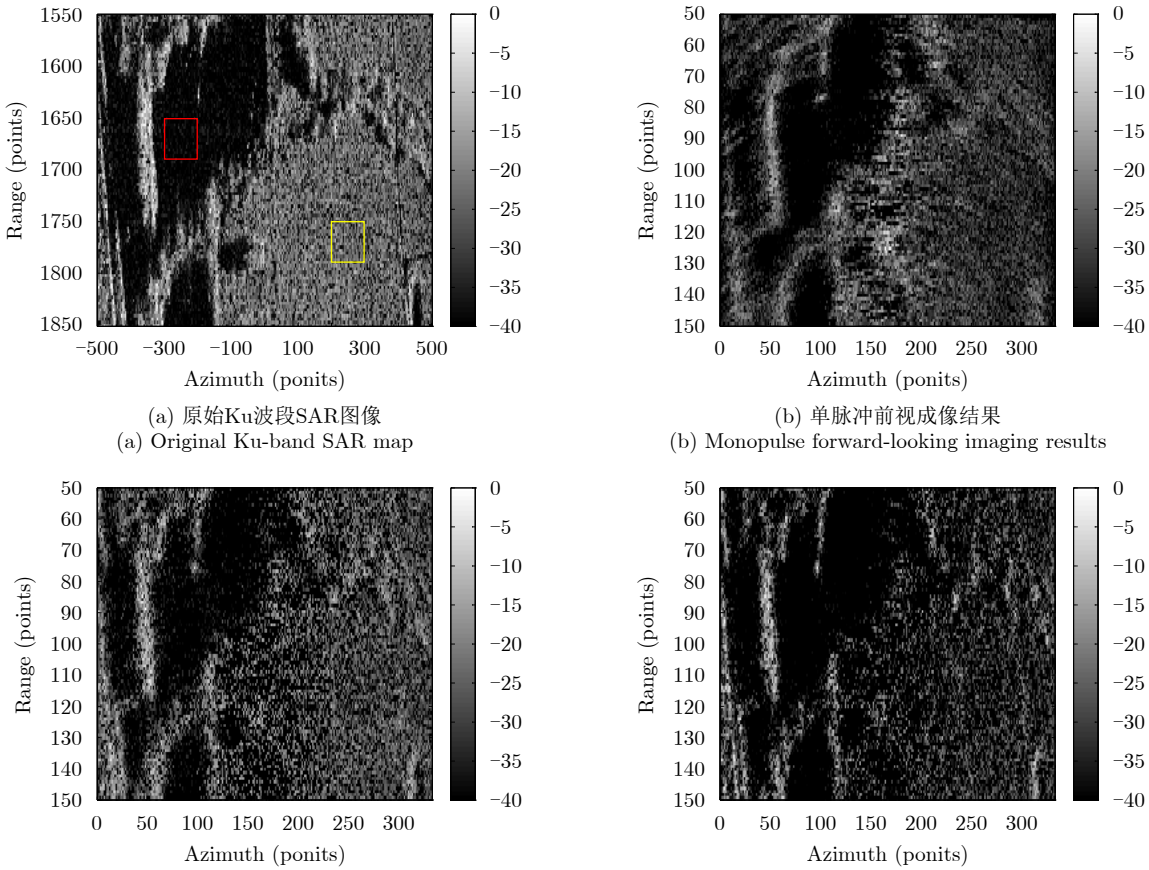

(a) 原始Ku波段SAR图像
(a) Original Ku-band SAR map

(b) 单脉冲前视成像结果
(b) Monopulse forward-looking imaging results

(c) 基于多普勒估计的单脉冲前视成像结果
(c) Monopulse forward-looking imaging results via Doppler estimates

(d) 基于重建多普勒估计的单脉冲成像结果
(d) Monopulse forward-looking imaging results via reconstructed Doppler estimates

图 6 仿真场景前视成像效果对比

Fig. 6 Comparison of experimental results in forward looking imaging

波束宽度约为2.5°。图7中每幅图右侧是场景中两个区域的局部放大图，右上为左侧场景岸边的图像，位于场景左侧–8°～0°附近；右下为水面一组点目标的图像，位于场景右侧12°附近。图7(a)为采用实孔径成像技术对雷达前视成像的结果，右侧水面目标的方位分布范围大，左侧岸边和陆地地貌轮廓模糊；图7(b)为采用传统单脉冲成像的结果，从右下侧点目标成像结果来看，目标强度增大，方位分布显著缩小，优于实孔径图像，说明了单脉冲成像有效地缩小了点目标扩展函数的方位分布范围，左侧陆地的成像结果则改善不明显，这是因为左侧场景为大块陆地，由对比度差异不明显的散射点组成，角闪烁导致的测角错误或测角结果异常使得图像模糊；图7(c)采用了基于多普勒估计的单脉冲前视成像算法，图7(d)则采用了基于重建和差通道多普勒估计的单脉冲前视成像算法，两种算法相对图7(b)对左侧陆地的成像效果都明显提升，表现为陆地场景的轮廓更清晰，纹理特征更丰富；从右下侧的局部放大图来看，对于水面目标，图7(c)成像后出现了少量的假目标，图7(d)则没有假目标；同时，也观察到采用多普勒处理后，在水面成像时，背景杂波相比图7(b)抬高了一些，这是由于多普勒处理时强目标的能量泄漏到其它多普勒分辨单元导致的。此外，图7(a)所示黄框对应位置作为所有图像截取的信号区域，红框对应位置作为所有图像截取的背景杂波区域，用于计算图像的统计SCR。实孔径图像的SCR约为29.49 dB，传统单脉冲成像图的统计SCR为28.49 dB；经过多普勒估计后的图7(c)和图7(d)的统计SCR分别为30.26 dB和30.30 dB，说明SCR得到了提高。

点目标仿真实验和实测数据成像实验表明：

(1) 对于前斜视方向同分辨单元内的多点目标，基于多普勒估计的单脉冲前视成像算法利用点目标之间的多普勒梯度差异分离目标，能有效解决角闪烁带来的图像模糊问题；

(2) 和差比幅测角后进行能量投影可以缩小点目标扩展函数的方位分布范围，而基于重建多普勒估计值进行和差比幅测角，能进一步提高测角精度，

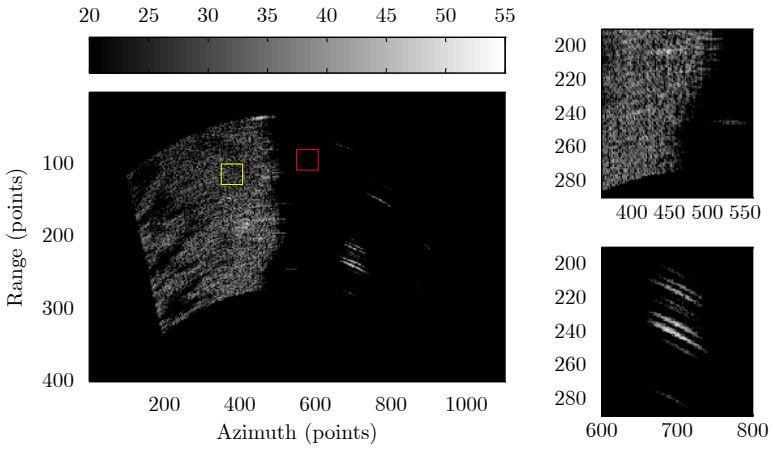

(a) 实孔径成像结果
(a) Real aperture image results

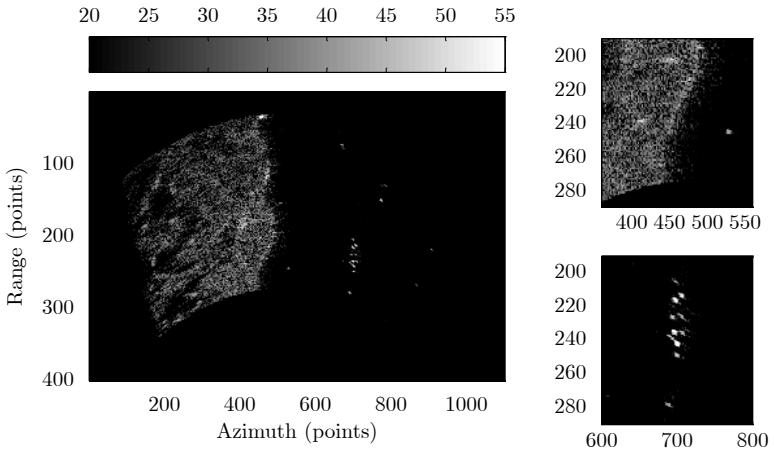

(b) 单脉冲前视成像结果
(b) Monopulse forward-looking imaging results

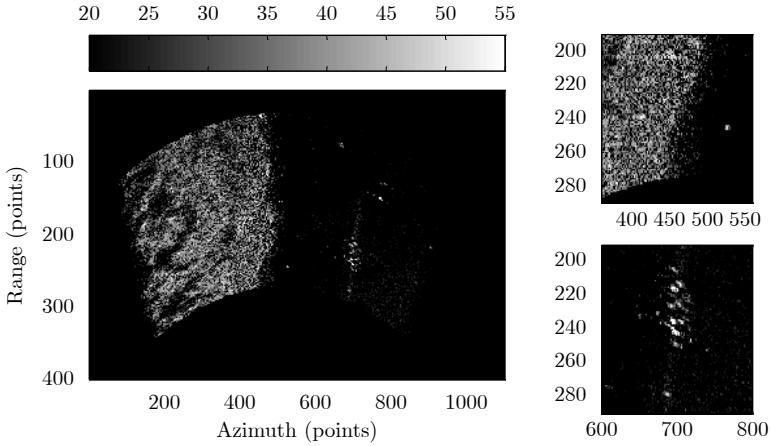

(c) 基于多普勒估计的单脉冲前视成像结果
(c) Monopulse forward-looking imaging results via Doppler estimates

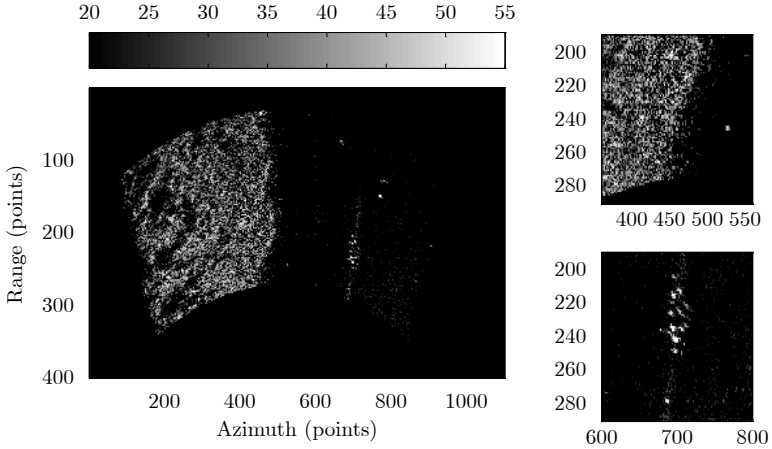

(d) 基于重建多普勒估计的单脉冲成像结果
(d) Monopulse forward-looking imaging results via reconstructed Doppler estimates

图 7 实测数据前视成像效果对比

Fig. 7 Comparison of experimental results in forward-looking imaging

减小点目标扩展函数的方位分布范围，从而提高图像清晰度。

5 结论

本文研究了基于单脉冲雷达和差通道多普勒估计的前视成像技术，对扫描雷达回波序列沿方位向分帧进行多普勒处理，实现了前斜视方向多目标的分辨，基于重建估计值的和差比幅测角则提高了对天线覆盖范围内目标的定位精度，仿真和实测数据验证了所提算法能有效提升前视图像的清晰度，使存在大量散射点的场景轮廓更清晰，纹理更丰富。由于多目标间的多普勒频差受到平台运动速度、目标相对运动方向的夹角以及雷达系统的波长等因素影响，测角精度的改善指标需要结合雷达系统参数和平台特性进行具体分析。对于同时出现在前视方向左右两侧的对称目标，在DBS技术中由于多普勒频率相同会出现“左右模糊”的问题，在单脉冲成像时，由于位于同分辨单元也无法分离，同时，由于多普勒梯度差异急剧下降，在正前视方向一定范围内仍存在盲区，这些都是未来研究工作中要继续关注的。

参 考 文 献

[1] 杨建宇. 雷达对地成像技术多向演化趋势与规律分析[J]. 雷达学报, 2019, 8(6): 669–692. doi: 10.12000/JR19099.
YANG Jianyu. Multi-directional evolution trend and law analysis of radar ground imaging technology[J]. *Journal of Radars*, 2019, 8(6): 669–692. doi: 10.12000/JR19099.

[2] ZHANG Yongchao, ZHANG Yin, HUANG Yulin, *et al*. Angular superresolution for scanning radar with improved regularized iterative adaptive approach[J]. *IEEE Geoscience and Remote Sensing Letters*, 2016, 13(6): 846–850. doi: 10.1109/LGRS.2016.2550491.

[3] 吴迪, 朱岱寅, 朱兆达. 机载雷达单脉冲前视成像算法[J]. 中国图象图形学报, 2010, 15(3): 462–469. doi: 10.11834/jig.20100317.
WU Di, ZHU Daiyin, and ZHU Zhaoda. Research on

nomopulse forward-looking imaging algorithm for airborne radar[J]. *Journal of Image and Graphics*, 2010, 15(3): 462–469. doi: 10.11834/jig.20100317.

[4] 吴迪, 朱岱寅, 田斌, 等. 单脉冲成像算法性能分析[J]. 航空学报, 2012, 33(10): 1905–1914.
WU Di, ZHU Daiyin, TIAN Bin, *et al*. Performance evaluation for monopulse imaging algorithm[J]. *Acta Aeronautica et Astronautica Sinica*, 2012, 33(10): 1905–1914.

[5] 吴迪, 杨成杰, 朱岱寅, 等. 一种用于单脉冲成像的自聚焦算法[J]. 电子学报, 2016, 44(8): 1962–1968. doi: 10.3969/j.issn.0372-2112.2016.08.027.
WU Di, YANG Chengjie, ZHU Daiyin, *et al*. An autofocusing algorithm for monopulse imaging[J]. *Acta Electronica Sinica*, 2016, 44(8): 1962–1968. doi: 10.3969/j.issn.0372-2112.2016.08.027.

[6] 李悦丽, 梁甸农, 黄晓涛. 一种单脉冲雷达多通道解卷积前视成像方法[J]. 信号处理, 2007, 23(5): 699–703. doi: 10.3969/j.issn.1003-0530.2007.05.013.
LI Yueli, LIANG Diannong, and HUANG Xiaotao. A multi-channel deconvolution based on forword-looking imaging method in monopulse radar[J]. *Signal Processing*, 2007, 23(5): 699–703. doi: 10.3969/j.issn.1003-0530.2007.05.013.

[7] 唐琳, 焦淑红, 齐欢, 等. 一种单脉冲雷达多通道L1正则化波束锐化方法[J]. 电子与信息学报, 2014, 36(9): 2201–2206. doi: 10.3724/SP.J.1146.2013.01792.
TANG Lin, JIAO Shuhong, QI Huan, *et al*. A new monopulse radar beam sharpening method with multichannel L1 regularization[J]. *Journal of Electronics & Information Technology*, 2014, 36(9): 2201–2206. doi: 10.3724/SP.J.1146.2013.01792.

[8] SHERMAN S M, BARTON D K, 周颖, 陈远征, 赵锋, 等译. 单脉冲测向原理与技术[M]. 2版. 北京: 国防工业出版社, 2013: 172–197.
SHERMAN S M, BARTON D K, ZHOU Ying, CHEN Yuanzheng, ZHAO Feng, *et al*. translation. Monopulse Principles and Techniques[M]. 2nd ed. Beijing: National Defense Industry Press, 2013: 172–197.

[9] ZHANG Xin, WILLETT P K, and BAR-SHALOM Y. Monopulse radar detection and localization of multiple unresolved targets via joint bin processing[J]. *IEEE Transactions on Signal Processing*, 2005, 53(4): 1225–1236. doi: 10.1109/TSP.2005.843732.

[10] 杨洋, 李悦丽. 单脉冲前视成像多目标分辨算法[J]. 信号处理, 2016, 32(9): 1055–1064. doi: 10.16798/j.issn.1003-0530.2016.09.07.
YANG Yang and LI Yueli. Multi-targets discrimination algorithm in monopulse forward-looking imaging[J]. *Journal of Signal Processing*, 2016, 32(9): 1055–1064. doi: 10.16798/j.issn.1003-0530.2016.09.07.

[11] LONG Teng, LU Zheng, DING Zegang, *et al*. A DBS Doppler centroid estimation algorithm based on entropy minimization[J]. *IEEE Transactions on Geoscience and Remote Sensing*, 2011, 49(10): 3703–3712. doi: 10.1109/TGRS.2011.2142316.

[12] ZHANG Shouhong, MA Changzheng, and CHEN Baixiao. Monopulse radar three-dimensional imaging of maneuvering targets[C]. SPIE 3545, International Symposium on Multispectral Image Processing, Wuhan, China, 1998: 193–196. doi: 10.1117/12.323634.

[13] LI Jian and STOICA P. An adaptive filtering approach to spectral estimation and SAR imaging[J]. *IEEE Transactions on Signal Processing*, 1996, 44(6): 1469–1484. doi: 10.1109/78.506612.

[14] 马长征, 张守宏. 超分辨在单脉冲雷达三维成像中的应用[J]. 西安电子科技大学学报, 1999, 26(3): 379–382. doi: 10.3969/j.issn.1001-2400.1999.03.027.
MA Changzheng and ZHANG Shouhong. Applications of super-resolution signal processing on monopulse radar three dimensional imaging[J]. *Journal of Xidian University*, 1999, 26(3): 379–382. doi: 10.3969/j.issn.1001-2400.1999.03.027.

[15] LIU Xiaocong and LI Yueli. Parameter estimation of narrowband radio frequency interference based on local refinement search in frequency domain[C]. 2015 IEEE International Conference on Communication Problem-Solving, Guilin, China, 2015: 145–148. doi: 10.1109/ICCPS.2015.7454112.

[16] CHEN Hongmeng, LI Ming, ZHANG Peng, *et al*. Resolution enhancement for Doppler beam sharpening imaging[J]. *IET Radar, Sonar & Navigation*, 2015, 9(7): 843–851. doi: 10.1049/iet-rsn.2014.0384.

[17] 孙泓波, 顾红, 苏卫民, 等. 机载脉冲多普勒雷达DBS成像实验研究[J]. 数据采集与处理, 2001, 16(4): 423–427. doi: 10.3969/j.issn.1004-9037.2001.04.007.
SUN Hongbo, GU Hong, SU Weimin, *et al*. Experimental research of DBS imaging based on airborne pulse Doppler radar[J]. *Journal of Data Acquisition & Processing*, 2001, 16(4): 423–427. doi: 10.3969/j.issn.1004-9037.2001.04.007.

[18] 毛士艺, 李少洪, 黄永红, 等. 机载PD雷达DBS实时成像研究[J]. 电子学报, 2000, 28(3): 32–34. doi: 10.3321/j.issn:0372-2112.2000.03.009.
MAO Shiyi, LI Shaohong, HUANG Yonghong, *et al*. Study of real-time image by DBS on airborne PD radar[J]. *Acta Electronica Sinica*, 2000, 28(3): 32–34. doi: 10.3321/j.issn:0372-2112.2000.03.009.

[19] 王娟, 赵永波. Keystone变换实现方法研究[J]. 火控雷达技术, 2011, 40(1): 45–51. doi: 10.3969/j.issn.1008-8652.2011.01.010.

WANG Juan and ZHAO Yongbo. Research on implementation of Keystone transform[J]. *Fire Control Radar Technology*, 2011, 40(1): 45–51. doi: 10.3969/j.issn.1008-8652.2011.01.010.

作 者 简 介

李悦丽(1973–)，女，湖南浏阳人，博士，国防科技大学电子科学学院教授。主要研究方向为机载雷达合成孔径成像、前视成像以及射频干扰抑制技术。
E-mail: liyueli4uwb@nudt.edu.cn

马萌恩(1996–)，男，陕西渭南人，国防科技大学电子科学学院硕士。主要研究方向为雷达信号处理与成像技术。
E-mail: mamengen18@nudt.edu.cn

赵崇辉(1979–)，男，河北鹿泉人，硕士，北京遥感设备研究所高工、型号主任设计师，主要研究方向为雷达总体设计、毫米波雷达成像。
E-mail: zhaochonghui@163.com

周智敏(1957–)，男，河北易县人，国防科技大学电子科学学院教授，主要研究方向为超宽带雷达技术。

Forward-looking Imaging via Doppler Estimates of Sum-difference Measurements in Scanning Monopulse Radar

LI Yueli*① MA Meng'en① ZHAO Chonghui*② ZHOU Zhimin①

①(*College of Electronic Science and Technology, National University of Defense Technology, Changsha* 410073, *China*)

②(*Science and Technology on Millimeter-wave Laboratory, Beijing* 100854, *China*)

Abstract: The monopulse technique is used in scanning radar systems to improve image quality in the forward-looking area. However, monopulse measurements fail to resolve multiple targets in the same resolution cell because of angular glint, and this often results in image blurring. We propose a monopulse forward-looking imaging method based on the Doppler estimates of sum-difference measurements. First, target multiplicity is resolved using the different Doppler shifts caused by the relative motion between the platform and the targets in different directions. High azimuthal angle measurement accuracy of the Doppler estimates is obtained using the Sum-Difference Amplitude-Comparison (SDAC) monopulse technique. Afterward, the intensity of the sum channel estimates is projected onto the image plane according to the range and angle measurements. To improve the precision of angle measurements, a Chirp-Z Transform (CZT)-based algorithm is proposed for the reconstruction of the Doppler estimates of the sum-difference channels. The simulation results demonstrate the capability of the proposed methods in resolving multiple targets at high squint angles in a large scanning field. Real data experiments show that the CZT-based algorithm significantly improved image profiles compared with the conventional monopulse imaging method.

Key words: Monopulse radar; forward-looking imaging; Sum-Difference Amplitude-Comparison (SDAC); Chirp-Z transform (CZT)

CLC index: TN958.4 **Document code**: A **Article number**: 2095-283X(2021)01-0131-13

DOI: 10.12000/JR20111

Reference format: LI Yueli, MA Meng'en, ZHAO Chonghui, *et al*. Forward-looking imaging via Doppler estimates of sum-difference measurements in scanning monopulse radar[J]. *Journal of Radars*, 2021, 10(1): 131–142. DOI: 10.12000/JR20111.

1 Introduction

High-resolution forward-looking imaging refers to the two-dimensional microwave imaging of the front view of an aircraft. The technology has recently garnered significant interest in the field of earth observation research. Presently, the main techniques for forward-looking imaging include bistatic Synthetic Aperture Radar (SAR) imaging, super-resolution imaging, and the Monopulse Technique (MT). The latter two can be used with monostatic radars, with a mechanical scanning antenna or a phased array. As the beam scans across the front scene, the azimuthal response signals can be modeled as the convolution of the antenna pattern and the Radar Cross Section (RCS) of the scatterers in the background. The super-resolution technique reconstructs the scene by deconvoluting the azimuthal echoes with a convolution kernel matrix that shifts the antenna pattern vector. Yang *et al.*[1,2] studied the theoretical model and implementation methods for angular super-resolution imaging and demonstrated several resolution improvements in airborne radar experiments. Wu *et al.*[3–5] studied monopulse imaging techniques based on the scanning mode, analyzing the resolution performance for specific scenarios and providing an

Manuscript received August 01, 2020; Revised October 27, 2020; Published online November 16, 2020

*Corresponding Author: LI Yueli, liyueli4uwb@nudt.edu.cn; ZHAO Chonghui, zhaochonghui@163.com

Foundation Items: The National Pre-Research Foundation (61404150103, 61425020604)

Corresponding Editor: ZHU Daiyin

autofocusing imaging algorithm. In Ref. [6], we studied a deconvolution algorithm based on the sum-difference channels of monopulse systems. As the sum-difference antenna patterns do not strictly fulfill the coprime condition, the deconvolution operation leads to noise amplification in the reconstructed results. Therefore, Tang *et al.*[7] introduced the ℓ_1 regularization constraints to effectively suppress high-frequency noise.

The Sum-difference Amplitude-Comparison (SDAC) technique, as a simultaneous lobing technique, measures the Direction-of-Arrival (DOA) of a target in the resolution bin using the amplitude-comparison ratio. Monopulse forward imaging, which does not require an ideal trajectory, is a practical method with low complexity. However, the process suffers from the catastrophic effects of target multiplicity owing to the freedom limit in the angular dimension, which is called "angular glint". The phenomenon results in angle measurement degradation and thus image blurring, especially for nonsparse scenes. Sherman *et al.*[8] systematically developed the theory of target multiplicity in monopulse radars. He indicated that in the traditional monopulse radar, two or more independent targets could not be resolved using the returned signals in a single pulse. However, if there are changes in beam pointing, frequency, or polarization between pulses, over two targets can be resolved[8]. A Maximum-Likelihood Extractor (MLE) has been developed to address target multiplicity through the joint bin processing of the monopulse radar. The target parameters are estimated using optimization algorithms to detect and resolve up to four targets falling between two consecutive sampling points in the main beam[9,10]. However, the computational complexity of the joint MLE is high, and the feasibility of real-time imaging is yet to be verified. The resolution of multiple targets in the Doppler domain according to their Doppler differences has also been proposed. This approach has been applied in the Doppler Beam Sharpen (DBS) technique to improve image resolution[11]. Chen *et al.*[12–14] developed the three-dimensional imaging technology of Inverse SAR (ISAR) by improving the resolution performance in the Doppler domain through super-resolution imaging. The amplitude and phase estimation algorithm achieved a higher Doppler resolution than the Fast Fourier Transform (FFT). Scanning radar forward-looking imaging based on DBS has the potential to solve angular ambiguity caused by multiple targets. However, overcoming the Doppler gradient descent between targets in the forward-looking area is still necessary.

To solve the problem of image degradation caused by the difficulty in distinguishing multiple targets in the MT, we propose a forward-looking imaging method based on the Doppler estimates of the sum-difference measurements in scanning radars. First, the Doppler centroid differences at different squint angles separate the targets in the same range cell. Then, SDAC is manipulated to measure the off-axis angle of the targets. Then, the intensity of the Doppler estimates of the sum channel is projected onto the imaging plane according to the range and angle measurements. The target's Doppler frequency accuracy significantly influences the angular precision; therefore, the sum-difference Doppler estimates are reconstructed using the Chirp-Z Transform (CZT)[15]: First, each Doppler unit in the main beam of the sum channel is refined using the CZT, and then the local maximum absolute value in the refined Doppler unit is searched to determine the accurate Doppler frequency of the target. Then, the sum-difference estimates are reconstructed according to the precise Doppler frequency. Finally, the estimates are used for SDAC and energy projection. Simulation and experimental results show that the proposed method, based on the reconstructed Doppler estimates, effectively improves the radar's ability to resolve multiple targets in highly squinted directions compared with the traditional monopulse forward-looking imaging algorithm. The method also improves the positioning accuracy of the scatterers and thus enhances image clarity.

2 Monopulse Forward-looking Imaging Based on Doppler Estimates

Suppose that a monopulse coherent radar mounted on a moving platform scans the forward-

looking scene at a uniform angular velocity, ω, and the radar Pulse Repetition Frequency (PRF) is f_{p}. After pulse compression and motion compensation, the sum-and-difference signal vectors of consecutive pulses in a range cell are respectively expressed as $\boldsymbol{y}_{\Sigma} = [y_{\Sigma 1}\ y_{\Sigma 2}\ \cdots\ y_{\Sigma N}]^{\mathrm{T}}$ and $\boldsymbol{y}_{\Delta} = [y_{\Delta 1}\ y_{\Delta 2}\ \cdots\ y_{\Delta N}]^{\mathrm{T}} \in \mathbb{C}_{N\times 1}$, where N is the pulse number in the Coherent Processing Interval (CPI). The signal model can be expressed as a matrix as follows:

$$\begin{cases} \boldsymbol{y}_{\Sigma} = \boldsymbol{A}_{\Sigma}\boldsymbol{s} + \boldsymbol{n}_{\Sigma} \\ \boldsymbol{y}_{\Delta} = \boldsymbol{A}_{\Delta}\boldsymbol{s} + \boldsymbol{n}_{\Delta} \end{cases} \tag{1}$$

where $\boldsymbol{s} \in \mathbb{C}_{K\times 1}$ denotes the RCS distribution of the scatterers at the uniform scanned grids; $\boldsymbol{A}_{\Sigma}, \boldsymbol{A}_{\Delta} \in \mathbb{C}_{N\times K}$ represent the steering matrices constituted by the spatial scanning antenna patterns of the sum–difference channels; and $\boldsymbol{n}_{\Sigma}, \boldsymbol{n}_{\Delta} \in \mathbb{C}_{N\times 1}$ are the independent additive noise vectors (for simplicity, the complex noise of each channel follows an independent Gaussian random process with mean zero and variance σ^2). Let $\theta_{3\mathrm{dB}}$ denote the 3 dB azimuth beamwidth; N indicates the number of dwell pulses transmitted and received by the radar at the azimuthal angle, θ_0; and $K = \lfloor \theta_{3\,\mathrm{dB}} f_{\mathrm{p}}/\omega \rfloor$ represents the number of pulses in the beam illumination interval; hence, $N \ll K$. Thus, Eq. (1) is underdetermined, and it is an ill-posed inverse problem. Because the antenna gain variation within the CPI is almost negligible, the azimuthal RCS distribution cannot be obtained from Eq. (1), owing to the singularity of the sample covariance matrix. Two technical approaches for forward-looking imaging are proposed to tackle the problem: an MT-based approach and the DBS technique. The MT-based approach involves measuring the off-axis angle of the scatterers through a comparison of the amplitudes or phases of the sum-difference samples. Generally, the MT can achieve a more precise angle measurement of a single scatterer than the main beam and then project the scatterer's energy onto the imaging plane[3]. Consequently, the method can significantly reduce the distribution width of a point scatterer's azimuthal Point Spread Function (PSF) and improve the image resolution. However, the MT fails to distinguish multiple scatterers in a resolution bin and can only measure their centroid[4]. In the DBS technique, the scatterers are separated according to the Doppler gradient difference generated by the relative motion between them and the platform. Doppler centroid estimation and clutter locking steps are used to obtain the azimuth angle of the scatterers in each Doppler unit, and energy is projected onto the imaging plane to achieve beam sharpening[16,17]. However, the sharpening ratio is limited by the Doppler filter bandwidth, f_{p}/N. Generally, the DBS can achieve 32 times higher azimuth resolution than the real-aperture imaging at squint angles of 30°∼50°. With increasing squint angle, the sharpening ratio will sharply decrease, owing to the decrease in the Doppler bandwidth of the ground clutter spectrum, and thus, the front view of a blind area will be formed[18].

This paper presents a forward-looking imaging method based on the sum-difference Doppler estimates of a monopulse radar. The process combines the above two technical approaches: First, Doppler processing is performed on the signal vectors across the range cell of the scanning radar. The Doppler differences are used to separate the scatterers in different Doppler units. Therefore, multitarget aliasing in the same resolution bin can be alleviated to improve the azimuthal resolution. Then, according to the Doppler estimates of the sum-difference channels, the SDAC is manipulated to obtain a precise angle measurement for each scatterer. Finally, the energy is projected according to the scattering location.

A signal model for angle measurement based on Doppler estimation is established for the beam scanning monopulse radar. Like Eq. (1), let the N samples in the same range cell constitute a one-dimensional uniform sampling vector of the return signals, and $\boldsymbol{a}_{\mathrm{D}}(\omega) \triangleq [1\ \mathrm{e}^{-\mathrm{j}\omega}\ \cdots\ \mathrm{e}^{-\mathrm{j}(N-1)\omega}]^{\mathrm{T}}$ denote the steering vector at the Doppler frequency, ω. Then, the uniform Doppler sampling interval, $\omega_n = 2\pi n/N, n = 0, 1, \cdots, N-1$, is normalized using the PRF. $\boldsymbol{A}_{\mathrm{D}} \triangleq [\boldsymbol{a}_{\mathrm{D}}(\omega_0)\ \boldsymbol{a}_{\mathrm{D}}(\omega_1)\ \cdots\ \boldsymbol{a}_{\mathrm{D}}(\omega_{N-1})] \in \mathbb{C}_{N\times N}$ is the Fourier-basis matrix equivalent to the Discrete Fourier Transform (DFT) across the slow time; that is,

$$\boldsymbol{A}_{\mathrm{D}}=\begin{bmatrix} 1 & 1 & \cdots & 1 \\ 1 & \mathrm{e}^{-\mathrm{j}\omega_1} & \cdots & \mathrm{e}^{-\mathrm{j}\omega_{N-1}} \\ \vdots & \vdots & \ddots & \vdots \\ 1 & \mathrm{e}^{-\mathrm{j}(N-1)\omega_1} & \cdots & \mathrm{e}^{-\mathrm{j}(N-1)\omega_{N-1}} \end{bmatrix},$$
$$\omega_n = 2\pi n/N, n = 0, 1, \cdots, N-1 \tag{2}$$

The Doppler estimates of the sum-difference channels can also be expressed as

$$\left.\begin{aligned} \boldsymbol{Y}_{\Sigma} &= \boldsymbol{A}_{\mathrm{D}}\boldsymbol{y}_{\Sigma} = \boldsymbol{A}_{\mathrm{D}}(\boldsymbol{A}_{\Sigma}\boldsymbol{s}+\boldsymbol{n}_{\Sigma}) = \boldsymbol{A}_{\mathrm{D}}\boldsymbol{A}_{\Sigma}\boldsymbol{s}+\boldsymbol{e}_{\Sigma} \\ \boldsymbol{Y}_{\Delta} &= \boldsymbol{A}_{\mathrm{D}}\boldsymbol{y}_{\Delta} = \boldsymbol{A}_{\mathrm{D}}(\boldsymbol{A}_{\Delta}\boldsymbol{s}+\boldsymbol{n}_{\Delta}) = \boldsymbol{A}_{\mathrm{D}}\boldsymbol{A}_{\Delta}\boldsymbol{s}+\boldsymbol{e}_{\Delta} \end{aligned}\right\} \tag{3}$$

DFT can be implemented using the FFT and $\boldsymbol{e}_{\Sigma}, \boldsymbol{e}_{\Delta} \in \mathbb{C}_{N\times 1}$ follow the Gaussian white noise distribution with mean zero. $N \ll K$ indicates that the antenna gain variation of each scatterer within the CPI can be ignored; the steering vectors $\boldsymbol{A}_{\Sigma}(\theta)$ and $\boldsymbol{A}_{\Delta}(\theta)$ are nearly unchanged for a scatterer $s(\theta)$. The scatterer azimuth angle can also be measured through a comparison of the amplitude of the sum-difference Doppler estimates after Doppler processing. Hence, if the Doppler frequency difference between different scatterers is more significant than f_{p}/N, Doppler processing can distinguish the scatterers and overcome target multiplicity.

First, the distribution width of clutter energy in the Doppler domain needs to be determined. This step is similar to clutter locking in DBS processing, and the Doppler centroid at the Line of Sight (LOS) and the Doppler bandwidth of the effective scattering within the 3 dB beam is calculated. As shown in the radar scanning imaging geometry in Fig. 1, the radar platform follows a uniform linear motion, with a forward flight speed v_x and a zero cross-track speed. The radar antenna beam scans the front area. Suppose that the current azimuth angle corresponding to the beam center of the channel antenna is θ, and the elevation angle is β; the Doppler centroid of the scattering corresponding to the LOS of the azimuthal beam is

$$f_{\mathrm{DC}} = \frac{2v_x\cos\theta\cos\beta}{\lambda} \tag{4}$$

where λ is the wavelength of the center frequency of the transmitted signal, and the unit index of the f_{DC} corresponding target is determined as $f_{\mathrm{DC}}/(f_{\mathrm{p}}/N)$. If the system is characterized by Doppler ambiguity, eliminating the influence of the Doppler ambiguity is necessary to achieve the correct index.

In the illumination area of the sum antenna beam, if an angle difference exists between the two targets, P1 and P2, in the same range cell (Fig. 1), the Doppler centroid difference Δf_{DC} can be defined as

$$\Delta f_{\mathrm{DC}} = f_{\mathrm{DC1}} - f_{\mathrm{DC2}} = = \frac{2v_x\cos\beta\left[\cos\theta - \cos(\theta+\Delta\theta)\right]}{\lambda} \tag{5}$$

The angle difference, $\Delta\theta$ is usually small, satisfying $\cos\Delta\theta \approx 1$, and $\sin\Delta\theta \approx \Delta\theta$; then, Δf_{DC} can be approximated as

$$\Delta f_{\mathrm{DC}} = \frac{2}{\lambda}\cdot v_x\sin\theta\cdot\cos\beta\cdot\Delta\theta \tag{6}$$

If the illuminated region of the 3 dB sum beamwidth on the ground plane is $\theta_{3\ \mathrm{dB}}$ and the influence of the Doppler rate is ignored, the Doppler bandwidth of the echoes from the resolution bin in the footprint becomes

$$\Delta f_{\mathrm{D}} \approx \frac{2}{\lambda}v_x\sin\theta\cdot\cos\beta\cdot\theta_{3\ \mathrm{dB}} \tag{7}$$

The distribution unit number of the RCS in the Doppler domain within the 3 dB beam is calculated as $\Delta f_{\mathrm{D}}/(f_{\mathrm{p}}/N)$. The clutter from the 3 dB beam in the Doppler domain is obtained using Eq. (7) and the Doppler centroid index determined by Eq. (4), and the corresponding Doppler unit indexes are obtained.

Suppose that the reflectivity of the scatterers in the 3 dB beam exists in several adjacent Dop-

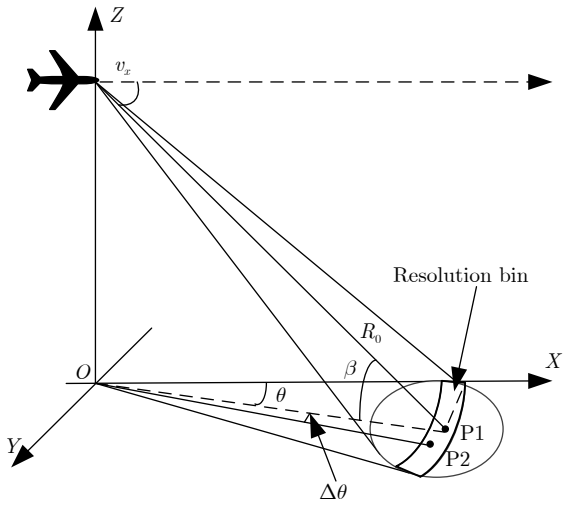

Fig. 1 Geometry of the forward-looking imaging of a scanning radar

pler units and $\boldsymbol{Y}_{\Sigma}(\omega_m)$ and $\boldsymbol{Y}_{\Delta}(\omega_m)$ are the Doppler estimates of the sum-difference channels in these units; the complex ratio of difference-to-sum channels, ε_m, is formulated as[8]

$$\varepsilon_m = \operatorname{sgn}\left(\boldsymbol{Y}_{\Sigma \mathrm{I}}(\omega_m)\boldsymbol{Y}_{\Delta \mathrm{I}}(\omega_m) + \boldsymbol{Y}_{\Sigma \mathrm{Q}}(\omega_m)\boldsymbol{Y}_{\Delta \mathrm{Q}}(\omega_m)\right) \cdot \frac{|\boldsymbol{Y}_{\Delta}(\omega_m)|}{|\boldsymbol{Y}_{\Sigma}(\omega_m)|}, \quad m = 0, 1, \cdots, M-1 \tag{8}$$

where sgn( ) represents the symbol operator, and subscripts I and Q denote the in-phase and quadrature parts of the received complex signals. According to the off-axis angle θ_e corresponding to the ε_m of the radar angle detection curve, the azimuth angle of the target is expressed as

$$\hat{\theta}_m = \theta - \theta_e \tag{9}$$

Finally, the estimated intensity of the sum Doppler unit is projected onto the imaging grid for energy accumulation to form the forward-looking image.

The flowchart of monopulse forward-looking imaging based on Doppler estimation is illustrated in Fig. 2. The raw data of the sum-difference channels are preprocessed through pulse compression. The keystone transform is used for range walk correction before azimuth processing[19]. The corrected echo signal in the same range cell is divided into frames across the azimuthal direction. Then, each frame of data is processed using the azimuthal FFT to estimate the Doppler components of the sum-difference channels. The Doppler unit indexes of the RCS distribution in the 3 dB beam are determined from the geometry and motion parameters. The monopulse complex ratio is calculated to estimate the angle of scatterers in the selected Doppler units. Finally, according to the range cell and direction of the scatterers, the intensity of the Doppler estimates in the sum main beam is projected onto the imaging plane to obtain the front-view image.

The monopulse forward-looking imaging (Fig. 2) is achieved through the projection of the target energy onto the imaging plane; thus, the position accuracy of the scatterers (including the range and azimuth measurements) plays a vital role in the imaging quality. The angle measurement accuracy achieved through SDAC is dependent on the Signal to Noise Ratio (SNR) of the echoes and the off-axis angle of the scatterer so that the performance does not considerably degrade with the increase in the squint angle relative to the zero Doppler range. Therefore, compared with the

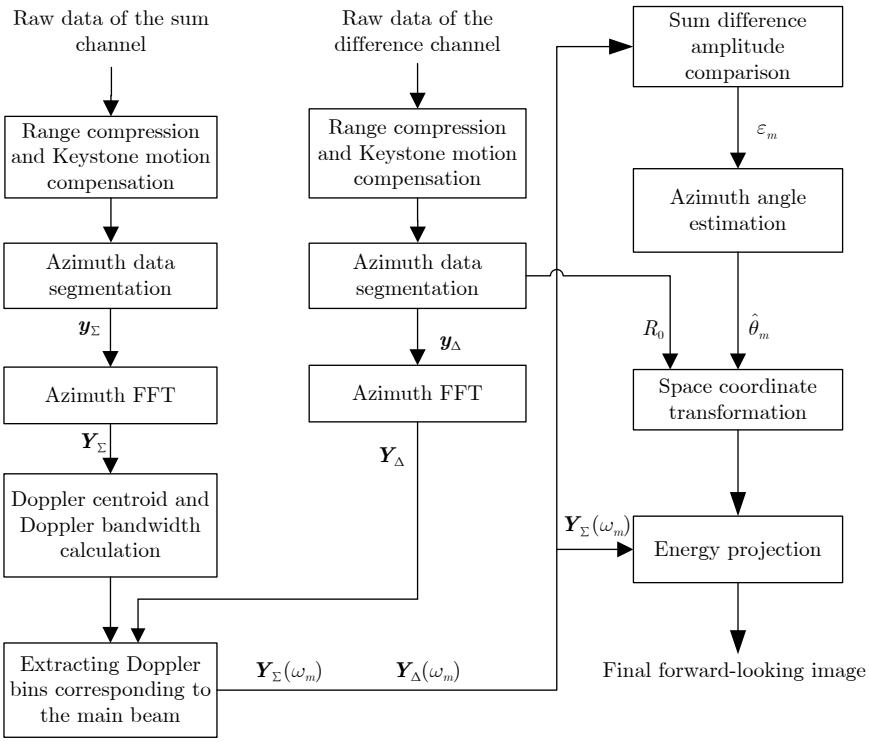

Fig. 2 Flowchart of mono pulse forward-looking imagination based on Doppler estimates

DBS technique, which is also based on Doppler processing, the monopulse forward-looking imaging can considerably improve the position precision of the scatterers, thereby improving image clarity.

3 Reconstruction of Sum-difference Channel Doppler Estimates for Monopulse Radar Based on CZT

FFT-based Doppler estimation of the sample vectors can separate the targets in the highly squinted directions in Section 2; however, the pulse number of CPI cannot be large owing to f_{p} and the phase error caused by platform motion. The resolution of the Doppler frequency constructed using DFT is not high enough in the forward-looking direction. Hence, the magnitude of a scatterer may be affected by side-lobes or energy leakage in the adjacent units, resulting in a sum-difference complex ratio error. A CZT-based Doppler estimation method is proposed to reconstruct the sum-difference Doppler estimates for a monopulse radar to improve the angular accuracy.

As indicated in Section 2, M Doppler units correspond to the scattering in the 3 dB beamwidth after Doppler processing. The Doppler centroid of the scatterer is re-estimated for each Doppler unit. The estimation is refined using the CZT at each Doppler unit to acquire a more precise Doppler frequency. The maximum local value is searched in the refined Doppler unit, and the corresponding frequency is set as the estimate of the actual Doppler centroid of the scatterer. For example, suppose that $\omega_m(i)$ is the Doppler frequency of the m^{th} refined Doppler unit;

$$\omega_m(i) = \omega_0 + i\frac{\Delta\omega}{L},\ m = 0,1,\cdots,M-1;\quad i = 0,1,\cdots,L-1 \tag{10}$$

where ω_0 denotes the starting frequency; $\Delta\omega$ denotes the Doppler increment; and L denotes the number of sampling points for sophisticated estimation. In this case, the local spectral resolution is $\Delta\omega/L$. Thus, the DFT of the response signal vector corresponding to Eq. (10) is

$$Y\left[\omega_m(i)\right] = \sum_{n=0}^{N-1} y(n)\mathrm{e}^{-\mathrm{j}\omega_m(i)n},\ i = 0,1,2,\cdots,L-1 \tag{11}$$

W is defined as

$$W = \mathrm{e}^{-\mathrm{j}\frac{\Delta\omega}{L}} \tag{12}$$

The refined estimates can be obtained using Eq. (11) and Eq. (12):

$$Y\left[\omega_m(i)\right] = \sum_{n=0}^{N-1} y(n)\mathrm{e}^{-\mathrm{j}\omega_0 n}W^{ni},\ i = 0,1,\cdots,L-1 \tag{13}$$

The superscript of W can be expanded as

$$ni = \frac{1}{2}\left[n^2 + i^2 - (i-n)^2\right] \tag{14}$$

Therefore, Eq. (13) can be expressed as follows:

$$Y\left[\omega_m(i)\right] = \sum_{n=0}^{N-1} y(n)\mathrm{e}^{-\mathrm{j}\omega_0 n}W^{n^2/2}W^{i^2/2}W^{-(i-n)^2/2},\quad i = 0,1,\cdots,L-1 \tag{15}$$

Let

$$g(n) = y(n)\mathrm{e}^{-\mathrm{j}\omega_0 n}W^{n^2/2},\quad n = 0,1,\cdots N \tag{16}$$

Eq. (15) can be recast as

$$Y\left[\omega_m(i)\right] = W^{i^2/2}\left[\sum_{n=0}^{N-1} g\left(n\right)W^{-(i-n)^2/2}\right],\quad i = 0,1,\cdots,L-1 \tag{17}$$

where $Y\left[\omega_m(i)\right]$ is the convolution of the sequences $g(n)$ and $W^{-n^2/2}$ multiplied by a factor $W^{i^2/2}$. $W^{-n^2/2}$ is a complex sequence varying with the linear increment $n\Delta\omega/L$; this means that the refined Doppler estimates of the sum channel $\boldsymbol{Y}_{\Sigma}\left(\omega_{mi}\right)$ can be calculated using the CZT. ω_{mr} denotes the actual Doppler centroid corresponding to the local peak. The Doppler estimate of the difference channel can be reconstructed according to the Doppler centroid ω_{mr}. First, the steering vector is defined as $\boldsymbol{a}_{\mathrm{D}}(\omega_{mr}) \triangleq [1\ \mathrm{e}^{-\mathrm{j}\omega_{mr}}\ \cdots\ \mathrm{e}^{-\mathrm{j}(N-1)\omega_{mr}}]^{\mathrm{T}}$. Multiplying the complex signal vector of the difference channel by the steering vector yields the Doppler estimate of the difference channel:

$$\boldsymbol{Y}_{\Delta}(\omega_{mr}) = \boldsymbol{a}_{\mathrm{D}}(\omega_{mr})^{\mathrm{T}}\boldsymbol{y}_{\Delta} \tag{18}$$

The steering vector used for reconstruction in Eq. (18) is the same as a column vector in the Fourier-basis matrix but has a more accurate Doppler centroid. Therefore, the sum-difference estimate is closer to the scatterer's actual value and can provide a more precise angle measurement. The sum-difference channel complex ratio

ε_{mr} is calculated from the reconstructed sum-difference Doppler estimates[8]:

$$\varepsilon_{mr}=\operatorname{sgn}\left(\boldsymbol{Y}_{\Sigma \mathrm{I}}(\omega_{mr})\,\boldsymbol{Y}_{\Delta \mathrm{I}}(\omega_{mr})+\boldsymbol{Y}_{\Sigma \mathrm{Q}}(\omega_{mr})\,\boldsymbol{Y}_{\mathrm{DQ}}(\omega_{mr})\right)\cdot\frac{|\boldsymbol{Y}_{\Delta}(\omega_{mr})|}{|\boldsymbol{Y}_{\Sigma}(\omega_{mr})|} \tag{19}$$

The off-axis angle of the scatterer is measured using the corresponding angle θ_e obtained from the sum–difference channel angle detection curve. The actual angle of the scatterer $\hat{\theta}_m$ is obtained according to Eq. (9).

The flowchart of the forward-looking imaging based on the reconstructed Doppler estimates is illustrated in Fig. 3. First, the original echoes of the sum-difference channels are processed. The keystone-corrected sum channel echoes are segmented into subframes of length N along the azimuth direction within the range cell. An FFT of the subframe data yields the Doppler estimation of the sum channel signals. The RCS distribution in the Doppler domain and the unit indexes are determined from the Doppler centroid and the Doppler bandwidth of the scattering within a 3 dB beam according to the motion parameters. The sum channel signals for each Doppler unit in the beam are processed using the CZT to refine the Doppler centroid estimation. The sum-difference estimates are reconstructed using a particular steering vector. The reconstructed data are used to calculate the complex monopulse ratio and measure the Doppler unit azimuth angle. Finally, the coordinate is transformed according to the range cell and the azimuth angle measurement, and the energy of the sum Doppler unit is projected onto the imaging plane.

4 Simulation and Experimental Results

4.1 Imaging simulation results for point targets array

The simulation parameters are presented in Tab. 1. Suppose that the radar sensor is mounted on an aircraft. It transmits coherent linear frequency-modulated signals with 1 μs pulse width and 50 MHz bandwidth. The center frequency of the transmitted signal is 18 GHz. The beam scans from –15° to 15°. The pulse number in the simulation is 2000. We set a scene containing 3×21 point targets in a 30 m × 30 m lattice. Each tar-

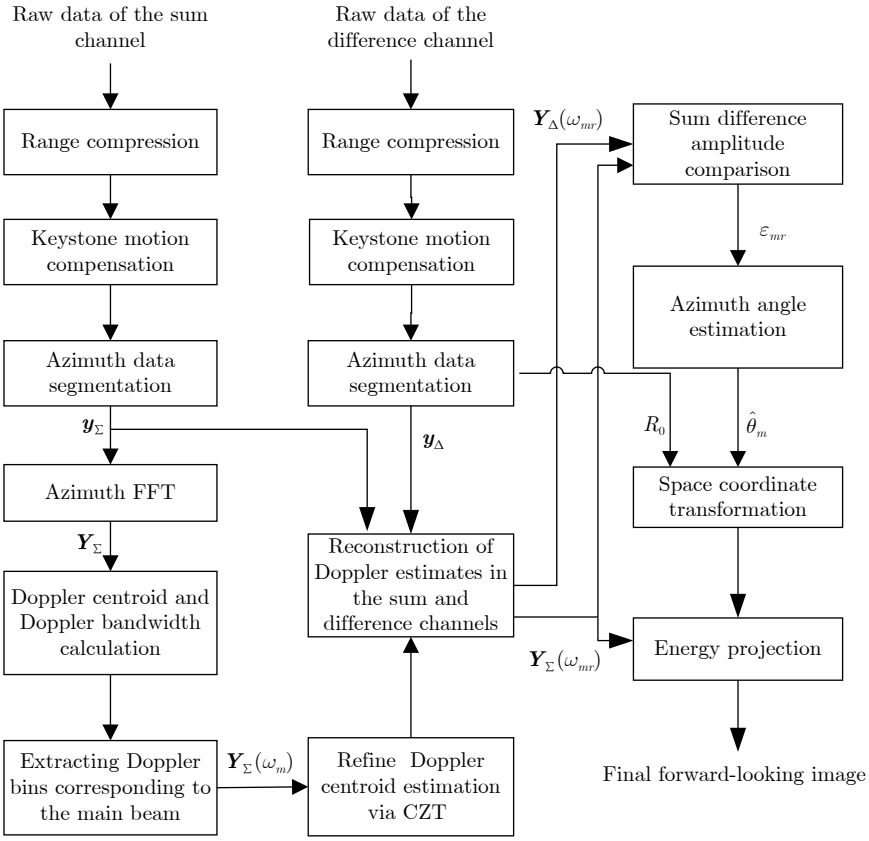

Fig. 3 Flowchart of monopulse forward-looking imaging based on the reconstructed Doppler estimates

get has a uniform intensity, and the axis of the scene center is (0, 1700) in meters on the ground surface. The SNR of the range-compressed data is set to 20 dB, and the noise follows a complex normal distribution with mean zero and variance σ^2.

After range compression and motion compensation, four methods are used for image formation, and the contour plots are illustrated in Fig. 4. As the cross-range resolution for DBS is low, the DBS images are not compared. The projection of the energy of the sum channel onto the ground plane results in the generation of a simulated real-aperture image, as shown in Fig. 4(a), which shows horizontal blurring owing to low cross-range resolution. Then, the sum-difference channel data are processed through the traditional monopulse imaging method (Fig. 4(b)). The scatterers are separated in the range dimension; however, they are horizontally blurred and connected in the azimuth direction. They cannot be accurately located, indicating the negative effect of target multiplicity on angle measurement using the MT. Fig. 4(c) and Fig. 4(d) present the results of imaging based on the procedures illustrated in Figs. 2 and 3, respectively. In the simulation, the pulse number of CPI is 64. In Fig. 4(c), point targets situated 200 m from the centerline of the scene are resolved, but the image quality is

Tab. 1 Simulation parameters of a forward-looking scanning radar

Parameters	Value	Parameters	Value
Center ground range	1700 m	Platform velocity	100 m/s
Center frequency	18 GHz	Pixel resolution	3 m × 3 m
Bandwidth	50 MHz	Pulse width	1 μs
3 dB beamwidth of the sum channel	5°	Antenna scanning area	–15°–15°
Pulse repeat frequency	2000 Hz	Scanning rate	30°/s

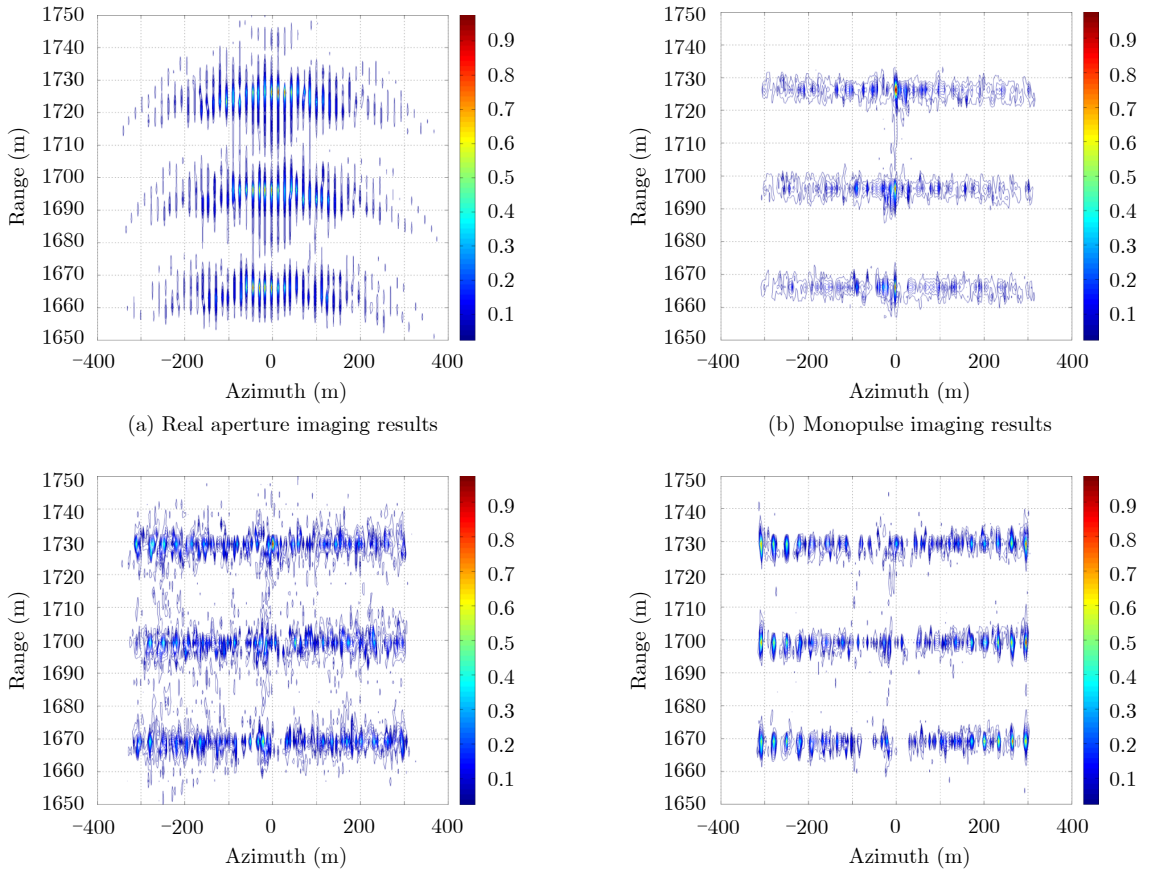

(a) Real aperture imaging results

(b) Monopulse imaging results

(c) Monopulse imaging results based on Doppler estimates by using FFT

(d) Monopulse imaging results based on reconstructed Doppler estimates by using CZT

Fig. 4 Comparison of forward-looking imaging performance (SNR = 20 dB)

poor because of the high background clutter. In contrast, the imaging results based on the CZT-reconstructed Doppler estimates narrow the azimuth PSFs of the scatterers, and the background clutter in the range-azimuth directions is also less severe than those in Fig. 4(c).

Fig. 5 compares the normalized azimuthal contour plots of the intensity distributions of 21 targets in Fig. 4(b)–Fig. 4(d) at the ground range of 1730 m. The red circles in the graph represent the actual azimuthal position and intensity of the point targets. The green dashed curve represents the azimuthal profile obtained using the traditional imaging algorithm; the curve shows that most targets are displaced from the right place. The blue dashed curve represents the profile processed using the FFT-based Doppler estimates; the target displacement is less severe than that of the traditional method, and the fluctuation and splitting of targets are apparent. The red curve represents the profile processed using the CZT-based Doppler estimates; the position of the point targets situated 180 m from the centerline of the scene agrees with the actual locations. The azimuthal PSF focuses well, and target intensity is uniform, showing significant improvements in the azimuthal resolution. An aliasing area exists around the centerline in both Figs. 4 and 5, owing to the decrease in the Doppler gradient with the increase in the squint angle. The method fails to resolve and locate multiple targets whose energy falls into the same Doppler unit.

4.2 Imaging results of extended targets

After demonstrating the validity of the proposed method in the reconstruction of a sparse scene, we test the application of the method in the reconstruction of an extended target. Because an extended target comprises numerous scatterers, it is much more difficult to reconstruct than a sparse scene owing to the occurrence of angular glint in the standard monopulse radar.

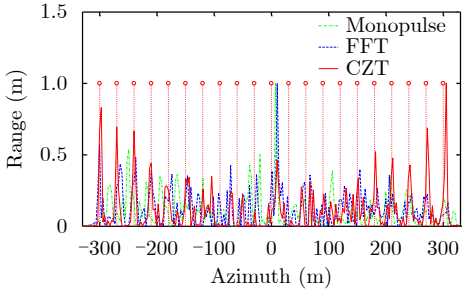

Fig. 5 Azimuthal contour plot for point targets at the range cell 1730 m (SNR = 20 dB)

We use a Ku-band SAR image to simulate the echoes of a forward-looking monopulse scanning radar in the simulation. The image data are downsampled to formulate an image with 3 m × 3 m pixel resolution (Fig. 6(a)). We consider the image as an extended target and locate it in a lattice, which is also centered at an axis [0 m, 1700 m] on the ground, with the maximum off-boresight angle of the scene at ∼17°; thus, the antenna scanning area is extended from −20° to 20° to ensure that the beam can cover the target. The echo data are generated according to the system parameters given in Tab. 1. The images are plotted in the dB scale. The energy of the sum channel data is projected on the ground plane to simulate an image using the traditional monopulse imaging method, as shown in Fig. 6(b), which features severe horizontal blurring due to angular glint. Then, the Doppler estimates of the sum-difference channel data are used to measure the DOA of scatterers within the beam footprint, and then the sum channel estimates are projected to form Fig. 6(c). The island outline is effectively reconstructed in the figure, and the scattering is generally consistent with that in Fig. 6(a). The imaging result in Fig. 6(d) is processed using the CZT-reconstructed Doppler estimates. Fig. 6(d) shows a more precise scene outline than Fig. 6(c), and the background clutter is also less severe than those in Fig. 6(c). The image quality is analyzed using the Signal to Clutter Ratio (SCR), a statistic that represents the ratio of the average target energy in a particular region to the average clutter energy in the background. The SCR in dB scale is defined as

$$\mathrm{SCR}=20\lg\left(\frac{S_\mathrm{r}}{C_\mathrm{r}}\right) \tag{20}$$

where S_r denotes the average signal amplitude in the yellow rectangular box, and C_r denotes the average clutter amplitude in the red rectangular box (Fig. 6(a)). Owing to the speckle noise, the

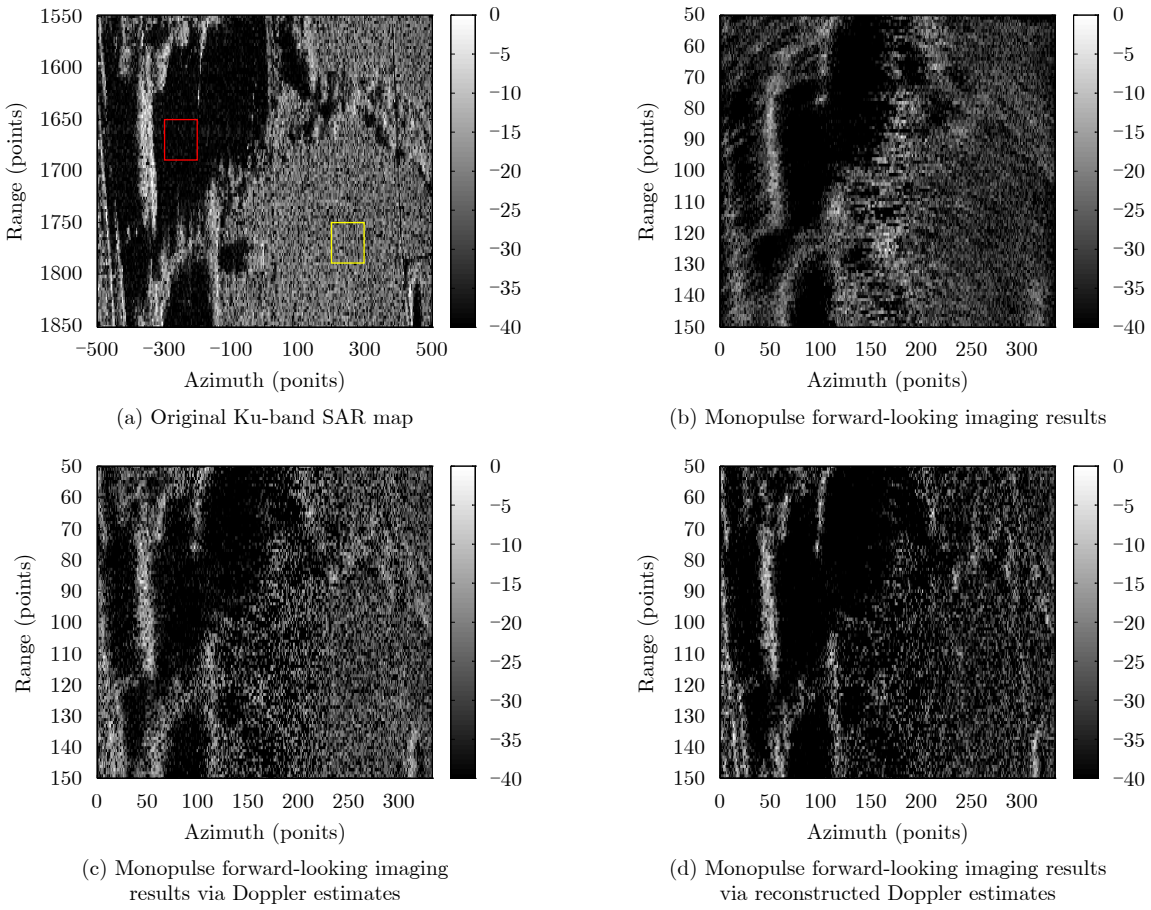

(a) Original Ku-band SAR map

(b) Monopulse forward-looking imaging results

(c) Monopulse forward-looking imaging results via Doppler estimates

(d) Monopulse forward-looking imaging results via reconstructed Doppler estimates

Fig. 6 Comparison of experimental results of forward-looking imaging

SCR in the original SAR map is ~20.03 dB, and the SCR in the same position in Fig. 6(b) is ~23.46 dB; however, Fig. 6(b) shows severe image distortion and a blurred outline of the extended target. The SCRs of Fig. 6(c) and Fig. 6(d) are 18.36 and 22.45 dB, respectively. In summary, the simulation results suggest that the proposed methods have the potential to image an extended target in a forward-looking scene.

4.3 Experimental results

Fig. 7 presents the forward-looking imaging results of experimental data obtained using an airborne monopulse radar system. The antenna scanned the water surface from –24° to 24° across the azimuth dimension in the flight. The antenna configuration was Sinc-shaped, with the 3 dB beamwidth equal to 2.5°. Fig. 7 presents the imagery results with two enlarged windows on the right side. The island profile located from –8° to 0° on the left part of the image is presented on the upper right end of the graph. A group of sparse targets on the water surface is presented on the lower-right end of the chart. Fig. 7(a) shows the real-aperture imaging results; the azimuth PSF of sparse targets on the water surface is extensive, and the profile of the island and the ground on the left region is blurred. Fig. 7(b) presents the imaging results obtained through traditional monopulse imaging. The cross-range resolution and the intensity of point targets on the water surface are improved, indicating the effectiveness of narrowing the PSF of sparse point targets. However, the left end of the image remains blurred, owing to angular glint caused by the significant number of identical scatterers in the resolution bin. Fig. 7(c) presents the imaging results from FFT-based Doppler estimates, and Fig. 7(d) shows the imaging results from CZT-based Doppler estimates. Both images' island profile at the left end is significantly improved and exhibits more texture characteristics. The enlarged local graphs at the lower-right end of the image show several artifact targets around the actual targets caused by energy leakage from neighboring strong

scatterers. This phenomenon is reduced using the CZT-based Doppler estimates (Fig. 7(d)). The signal and clutter regions are the red and yellow rectangular boxes in Fig. 7(a), respectively, used to calculate the SCR. The SCR of the real-aperture imaging result is ∼29.49 dB, and the SCR of the traditional monopulse imagery is ∼28.49 dB. According to Doppler estimates, the SCRs of Fig. 7(c) and Fig. 7(d) are 30.26 dB and 30.30 dB, respectively. The experimental results verify the effectiveness of the proposed method for SCR enhancement.

The simulation and experimental imaging results show the following:

(1) The monopulse forward-looking imaging based on Doppler estimation uses the Doppler gradient difference between point targets to separate the multiple point targets in the same resolution bin in the forward-looking direction, effectively solving the image blurring problem caused by angular glint;

(2) Energy projection after SDAC can narrow the azimuthal PSF of the scatterers. Doppler estimate reconstruction and SDAC can improve the angular measurement accuracy, thereby reducing the PSF and improving image clarity.

5 Conclusion

This study investigated the forward-looking imaging method based on Doppler estimates in standard monopulse radar systems. Doppler processing across the azimuth dimension allowed for the resolution of multiple targets in highly squinted directions. SDAC, based on reconstructed Doppler estimates, improved the angular accuracy of the scatterers. The simulation and experimental results demonstrated the validity of the proposed method for front-view imaging. The profile of the extended targets was more precise than those acquired through the traditional method, and the image texture details were enriched. The Doppler centroid difference between targets was

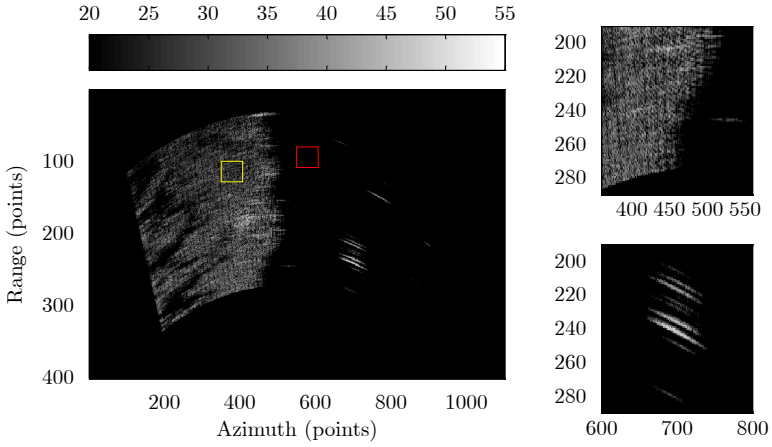

(a) Real aperture image results

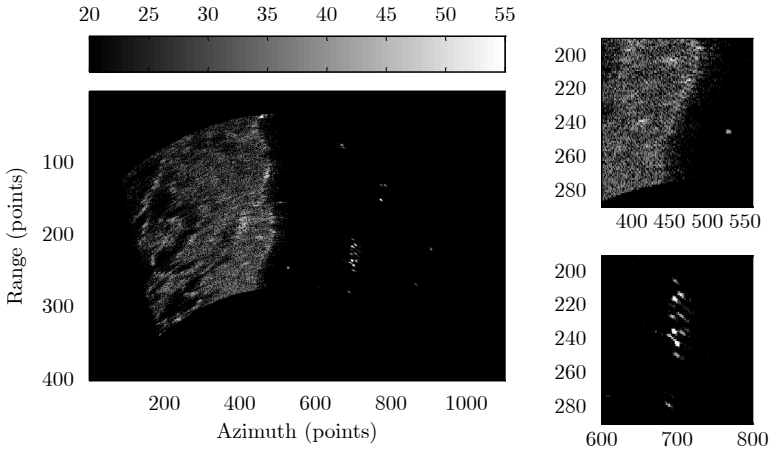

(b) Monopulse forward-looking imaging results

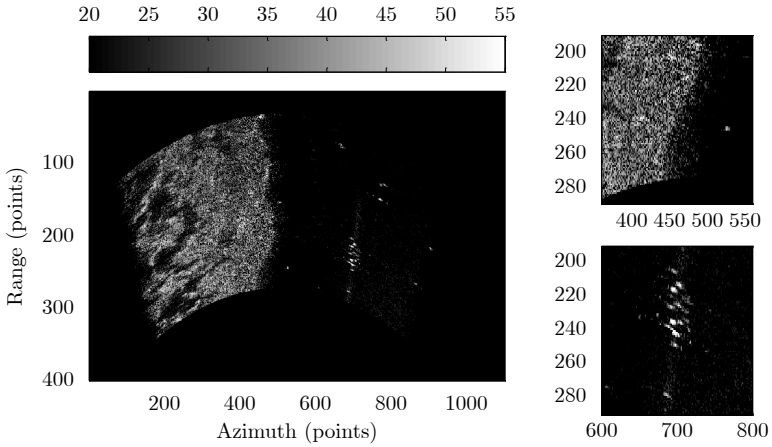

(c) Monopulse forward-looking imaging results via Doppler estimates

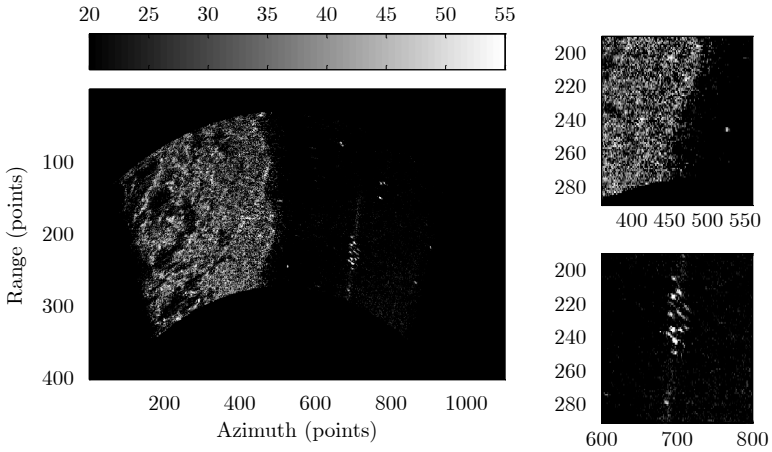

(d) Monopulse forward-looking imaging results via reconstructed Doppler estimates

Fig. 7 Comparison of experimental results in forward-looking imaging

affected by the platform velocity, the azimuth and elevation angles relevant to the flight path, and the wavelength of the transmitted signals. Therefore, for a specific case, resolution improvement needs to be analyzed according to the radar parameters and the platform property. However, if Doppler processing cannot resolve closely spaced targets, the method may not improve the cross-range resolution of the scene, which is a problem that needs to be tackled in future research.

References

[1] YANG Jianyu. Multi-directional evolution trend and law analysis of radar ground imaging technology[J]. *Journal of Radars*, 2019, 8(6): 669–692. doi: 10.12000/JR19099.

[2] ZHANG Yongchao, ZHANG Yin, HUANG Yulin, *et al*. Angular superresolution for scanning radar with improved regularized iterative adaptive approach[J]. *IEEE Geoscience and Remote Sensing Letters*, 2016, 13(6): 846–850. doi: 10.1109/LGRS.2016.2550491.

[3] WU Di, ZHU Daiyin, and ZHU Zhaoda. Research on nomopulse forward-looking imaging algorithm for airborne radar[J]. *Journal of Image and Graphics*, 2010, 15(3): 462–469. doi: 10.11834/jig.20100317.

[4] WU Di, ZHU Daiyin, TIAN Bin, *et al*. Performance evaluation for monopulse imaging algorithm[J]. *Acta Aeronautica et Astronautica Sinica*, 2012, 33(10): 1905–1914.

[5] WU Di, YANG Chengjie, ZHU Daiyin, *et al*. An autofocusing algorithm for monopulse imaging[J]. *Acta Electronica Sinica*, 2016, 44(8): 1962–1968. doi: 10.3969/j.issn.0372-2112.2016.08.027.

[6] LI Yueli, LIANG Diannong, and HUANG Xiaotao. A multichannel deconvolution based on forword-looking imaging method in monopulse radar[J]. *Signal Processing*, 2007, 23(5): 699–703. doi: 10.3969/j.issn.1003-0530.2007.05.013.

[7] TANG Lin, JIAO Shuhong, QI Huan, *et al*. A new monopulse radar beam sharpening method with multichannel L1 regularization[J]. *Journal of Electronics & Information Technology*, 2014, 36(9): 2201–2206. doi: 10.3724/SP.J.1146.2013.01792.

[8] SHERMAN S M, BARTON D K, ZHOU Ying, CHEN

Yuanzheng, ZHAO Feng, *et al.* translation. Monopulse Principles and Techniques[M]. 2nd ed. Beijing: National Defense Industry Press, 2013: 172–197.

[9] ZHANG Xin, WILLETT P K, and BAR-SHALOM Y. Monopulse radar detection and localization of multiple unresolved targets via joint bin processing[J]. *IEEE Transactions on Signal Processing*, 2005, 53(4): 1225–1236. doi: 10.1109/TSP.2005.843732.

[10] YANG Yang and LI Yueli. Multi-targets discrimination algorithm in monopulse forward-looking imaging[J]. *Journal of Signal Processing*, 2016, 32(9): 1055–1064. doi: 10.16798/j.issn.1003-0530.2016.09.07.

[11] LONG Teng, LU Zheng, DING Zegang, *et al.* A DBS Doppler centroid estimation algorithm based on entropy minimization[J]. *IEEE Transactions on Geoscience and Remote Sensing*, 2011, 49(10): 3703–3712. doi: 10.1109/TGRS.2011.2142316.

[12] ZHANG Shouhong, MA Changzheng, and CHEN Baixiao. Monopulse radar three-dimensional imaging of maneuvering targets[C]. SPIE 3545, International Symposium on Multispectral Image Processing, Wuhan, China, 1998: 193–196. doi: 10.1117/12.323634.

[13] LI Jian and STOICA P. An adaptive filtering approach to spectral estimation and SAR imaging[J]. *IEEE Transactions on Signal Processing*, 1996, 44(6): 1469–1484. doi: 10.1109/78.506612.

[14] MA Changzheng and ZHANG Shouhong. Applications of super-resolution signal processing on monopulse radar three dimensional imaging[J]. *Journal of Xidian University*, 1999, 26(3): 379–382. doi: 10.3969/j.issn.1001-2400.1999.03.027.

[15] LIU Xiaocong and LI Yueli. Parameter estimation of narrowband radio frequency interference based on local refinement search in frequency domain[C]. 2015 IEEE International Conference on Communication Problem-Solving, Guilin, China, 2015: 145–148. doi: 10.1109/ICCPS.2015.7454112.

[16] CHEN Hongmeng, LI Ming, ZHANG Peng, *et al.* Resolution enhancement for Doppler beam sharpening imaging[J]. *IET Radar, Sonar & Navigation*, 2015, 9(7): 843–851. doi: 10.1049/iet-rsn.2014.0384.

[17] SUN Hongbo, GU Hong, SU Weimin, *et al.* Experimental research of DBS imaging based on airborne pulse Doppler radar[J]. *Journal of Data Acquisition & Processing*, 2001, 16(4): 423–427. doi: 10.3969/j.issn.1004-9037.2001.04.007.

[18] MAO Shiyi, LI Shaohong, HUANG Yonghong, *et al.* Study of real-time image by DBS on airborne PD radar[J]. *Acta Electronica Sinica*, 2000, 28(3): 32–34. doi: 10.3321/j.issn:0372-2112.2000.03.009.

[19] WANG Juan and ZHAO Yongbo. Research on implementation of Keystone transform[J]. *Fire Control Radar Technology*, 2011, 40(1): 45–51. doi: 10.3969/j.issn.1008-8652.2011.01.010.

LI Yueli was born in Hunan, China, in 1973. She received the Bachelor's degree in communication engineering, and the Ph.D. degree in information and communication engineering from the National University of Defense Technology, Changsha, China, in 1995 and 2008, respectively. She is currently a full professor with the College of Electronic Science, National University of Defense Technology. Her research interests include radar signal processing, SAR imaging algorithms, forward-looking imaging principles, and radio frequency interference suppression.

MA Meng'en was born in Shanxi, China, in 1996. He received the Master's degree in information and communication engineering from the National University of Defense Technology, Changsha, China, in 2021. His research interests include radar signal processing and imaging algorithms.

ZHAO Chonghui was born in Hebei, China, in 1979. He received the Master's degree in telecommunications engineering from Harbin-Engineering-University, Harbin, China, in 2004. He has been with the Science and Technology on Milimeter-wave Laboratory, Beijing since 2006. His current research interests include radar system design and radar imaging.

ZHOU Zhimin was born in Hubei, China, in 1957. He received the Bachelor's degree in electronics engineering, and the Ph.D. degree in information and communication engineering from the National University of Defense Technology, Changsha, China, in 1982 and 2003, respectively. He is currently a professor at the National University of Defense Technology. His research fields include radar system design and ultra-wide-band radar technology.